J Sci Comput (2012) 53:150–193
DOI 10.1007/s10915-012-9602-y

The Method of Difference Potentials for the Helmholtz Equation Using Compact High Order Schemes

M. Medvinsky · S. Tsynkov · E. Turkel

Received: 4 October 2011 / Revised: 16 April 2012 / Accepted: 1 May 2012 /
Published online: 17 May 2012

Abstract The method of difference potentials was originally proposed by Ryaben'kii and can be interpreted as a generalized discrete version of the method of Calderon's operators in the theory of partial differential equations. It has a number of important advantages; it easily handles curvilinear boundaries, variable coefficients, and non-standard boundary conditions while keeping the complexity at the level of a finite-difference scheme on a regular structured grid. The method of difference potentials assembles the overall solution of the original boundary value problem by repeatedly solving an auxiliary problem. This auxiliary problem allows a considerable degree of flexibility in its formulation and can be chosen so that it is very efficient to solve.

Compact finite difference schemes enable high order accuracy on small stencils at virtually no extra cost. The scheme attains consistency only on the solutions of the differential equation rather than on a wider class of sufficiently smooth functions. Unlike standard high order schemes, compact approximations require no additional boundary conditions beyond those needed for the differential equation itself. However, they exploit two stencils—one applies to the left-hand side of the equation and the other applies to the right-hand side of the equation.

Dedicated to our friend Saul Abarbanel on the occasion of his 80th birthday.

M. Medvinsky · E. Turkel
School of Mathematical Sciences, Tel Aviv University, Ramat Aviv, Tel Aviv 69978, Israel

M. Medvinsky
e-mail: medvinsk@post.tau.ac.il
url: http://www.tau.ac.il/~medvinsk/

E. Turkel
e-mail: turkel@post.tau.ac.il
url: http://www.math.tau.ac.il/~turkel/

M. Medvinsky · S. Tsynkov (✉)
Department of Mathematics, North Carolina State University, Box 8205, Raleigh, NC 27695, USA
e-mail: tsynkov@math.ncsu.edu
url: http://www.math.ncsu.edu/~stsynkov

We shall show how to properly define and compute the difference potentials and boundary projections for compact schemes. The combination of the method of difference potentials and compact schemes yields an inexpensive numerical procedure that offers high order accuracy for non-conforming smooth curvilinear boundaries on regular grids. We demonstrate the capabilities of the resulting method by solving the inhomogeneous Helmholtz equation with a variable wavenumber with high order (4 and 6) accuracy on Cartesian grids for non-conforming boundaries such as circles and ellipses.

Keywords Difference potentials · Boundary projections · Calderon's operators · Regular grids · Curvilinear boundaries · Variable coefficients · Compact differencing · High order accuracy

1 Introduction

We propose a high order singularity-free methodology for the numerical solution of two- and three-dimensional boundary value problems of field and wave analysis. It applies to a wide variety of physical formulations (acoustic and electromagnetic wave transmission and scattering, heat transfer, linear elasticity, electro- and magnetostatics, Stokes flows, etc.). For definiteness, in this paper we illustrate the methodology by solving scalar wave propagation problems in the frequency domain.

1.1 Numerical Approximation of Differential Equations: Standard vs. Compact Differencing

Finite difference (FD) methods were historically the first methodology for the numerical solution of differential equations [39, 43]. They still remain a very powerful tool, and for smooth solutions on regular domains/grids lead to inexpensive and efficient algorithms. Their shortcoming is in dealing with more complicated geometries and solutions with low regularity. The issue of geometry is somewhat alleviated by the immersed boundary and related methods [29, 33]. The finite element method (FEM) and its extensions are also well established and powerful. Their strength is in dealing with complex geometries and low regularity of the solutions.

In practical problems of wave propagation though, especially in 3D, both FD and FEM have serious limitations because of their relatively high "points-per-wavelength" requirement, as well as numerical dispersion and, more generally, numerical pollution [1, 4, 23, Sect. 4.6.1]. The numerical phase velocity of the wave in these methods depends on the wavenumber k, so a propagating packet of waves with different frequencies gets distorted in the simulation. Furthermore, the numerical error strongly depends on k and this kind of error is inherent in FEM/FD. The error is proportional to $h^p k^{p+1}$, where p is the order of accuracy of the scheme. So the number of points per wavelength needed for a given accuracy behaves like $k^{1/p}$. Hence, for higher order accurate schemes the pollution effect is reduced. On the other hand, classical higher order FD or FEM methods require an extended stencil which complicates the boundary treatment.

Higher order accuracy can be achieved without expanding the stencil in schemes known as Collatz "Mehrstellen" [10], equation-based and related compact schemes [2, 3, 5, 6, 20, 31, 47, 48, 51] and Trefftz-FLAME [54]. Such schemes rely on a targeted approximation of the class of *solutions* rather than of a much broader class of generic sufficiently smooth functions. This does not imply any loss of generality though, because according to the Lax

theorem, for convergence one does not need to have consistency on functions which are not solutions.

Equation-based compact schemes use the equation itself to eliminate the distant stencil points. The classical Lax-Wendroff scheme [27] can be considered as early example of compact differencing, see Sect. 2.1. These high order schemes reduce pollution while keeping the treatment of the boundary conditions simple, because usually the order of the resulting difference equation is equal to the order of the differential equation. Hence, no additional numerical boundary conditions are required. However, the geometry of boundaries still remains a hurdle.

In FEM, on the other hand, a high order approximation can be built for arbitrary boundaries, but only in fairly sophisticated and costlier algorithms with isoparametric elements [50]. Besides, high order accuracy typically requires additional degrees of freedom, which entails an additional computational cost.

1.2 Reduction to Integral Equations

In traditional boundary element methods (BEM), linear boundary value problems are transformed into integral equations with respect to equivalent boundary sources, and the latter are subsequently discretized. Practical applications of such methods date back to the 1960s. They impose no limitations on the shape of the boundary and automatically account for the correct far field behavior of the solution

The matrices that appear in the context of BEM are usually full, as opposed to the sparse FD and FEM matrices. Significant progress in fast multipole methods (FMM) [18] has helped alleviate this issue. The treatment of the boundary conditions in BEM requires care, on a case-by-case basis, in the choice of the equivalent boundary sources, so that the resulting Fredholm equation is of the second kind (well-posed) rather than first. The evaluation of singular integrals may present problems in practice, especially in the vicinity of the boundary. The most serious shortcoming of BEM though is that these methods require explicit knowledge of the fundamental solution of the corresponding differential operator and hence, in practice, are limited to constant coefficients, i.e., to homogeneous media.

1.3 The Method of Difference Potentials

The objective of this paper is to construct a high order method that offers the geometric flexibility of BEM, yet is not limited to constant coefficients and does not involve singular integrals. At the same time, we avoid introducing additional unknowns, e.g., Lagrange multipliers that enforce weak continuity. Hence, we approximate the solution on the domain using high order finite differences on regular grids. The narrower the approximating space the better, so the preference is for compact equation-based schemes [20, 47].

Nevertheless, the shape of the domain may be arbitrary (yet smooth). To handle general boundaries not aligned with the grid, we employ Ryaben'kii's *method of difference potentials* [41, 42] further developed by Reznik [38], Sofronov [49], Kamenetskii [24–26], Tsynkov [57], and others. This approach applies to a given discretization on a regular structured grid and allows non-conforming curvilinear boundaries with no loss of accuracy. The method of difference potentials can be viewed as a discrete analogue of the method of Calderon's potentials and Calderon's boundary equations with projections in the qualitative theory of partial differential equations [7, 42, 46].

Prior developments of the method of difference potentials were done for standard non-compact schemes. Hence, the analysis in the current paper focuses on extending the method

to equation-based approximations that use an additional stencil operating on the data. The extension requires the proper definitions of difference potentials and projections, and involves extra steps needed to account for the source term of the equation.

The method of difference potentials has the following key advantages:

- *Maximum generality of boundary conditions*. The entire class of functions satisfying the underlying differential equation (with the boundary conditions yet unspecified) is characterized by an equivalent boundary equation (Calderon's boundary equation with projection). Only later are specific boundary conditions imposed. Any type of boundary conditions can be handled with equal ease, including mixed, nonlocal, interfaces, etc.
- The problem can be discretized on a regular structured grid, yet *the boundary can have an arbitrary shape* and need not conform to the grid. This causes no loss of accuracy due to staircasing [8, 22].
- Boundary representations inherit the accuracy of the core discretization on the regular grid. Hence, *high order approximations for problems with curved boundaries can be easily obtained.*
- *Variable coefficients* or equivalently, *heterogeneous media,* can be handled as easily as constant coefficients. The constructs of Calderon's operators stay essentially unchanged.
- The methodology *does not require numerical approximation of singular integrals.* Inverse operators used for computing the discrete counterparts to Calderon's potentials and projections involve no convolutions and no singularities and allow fast numerical computation.
- *Well-posedness of the discrete problem is guaranteed*. There is no need to be concerned with Fredholm equations of the first or second kind.

1.4 Outline of the Paper

In Sect. 2, we provide a brief account of the compact high order equation-based schemes [20, 47] for solving the variable coefficient Helmholtz equation. In Sect. 3, we introduce continuous Calderon operators and their discrete counterparts—difference potentials and projections, discuss their key properties, and show how the discrete constructs apply to compact high order schemes. In Sect. 4, we describe the resulting computational algorithm for the variable coefficient Helmholtz equation that handles general non-conforming boundaries on regular grids. *In particular, Sect. 4.5 contains a detailed step-by-step explanation of the numerical procedure in the form of a list of items to be performed in the given order*. In Sect. 5, we present results of computations confirming the high order accuracy for non-conforming boundaries. Finally, Sect. 6 contains conclusions and a discussion of future work.

2 Compact High Order Accurate Equation-Based Schemes

2.1 Example: The Lax-Wendroff Scheme

We provide a derivation of the classical Lax-Wendroff scheme that allows one to interpret it as an equation-based compact approximation.

Consider the simplest one-dimensional inhomogeneous advection equation:

$$\frac{\partial u}{\partial t} + \frac{\partial u}{\partial x} = f(x,t), \tag{1}$$

and introduce uniform grids of variables x and t with the sizes h and τ, respectively:

$$x_i = ih, \quad i = 0, \pm 1, \pm 2, \ldots,$$
$$t^p = p\tau, \quad p = 0, 1, 2, \ldots.$$

The explicit scheme

$$\frac{u_i^{p+1} - u_i^p}{\tau} + \frac{u_{i+1}^p - u_{i-1}^p}{2h} = f_i^p, \tag{2}$$

where $f_i^p \equiv f(x_i, t^p)$, is consistent for (1) with order $\mathcal{O}(\tau + h^2)$, because for any sufficiently smooth function $u = u(x,t)$ we can write using Taylor's formula:

$$\frac{u(x_i, t^{p+1}) - u(x_i, t^p)}{\tau} = \frac{\partial u}{\partial t}(x_i, t^p) + \frac{\tau}{2}\frac{\partial^2 u}{\partial t^2}(x_i, t^p) + \mathcal{O}(\tau^2) \tag{3a}$$

and

$$\frac{u(x_{i+1}, t^p) - u(x_{i-1}, t^p)}{2h} = \frac{\partial u}{\partial x}(x_i, t^p) + \frac{h^2}{6}\frac{\partial^3 u}{\partial x^3}(x_i, t^p) + \mathcal{O}(h^3). \tag{3b}$$

Since we have $\mathcal{O}(h^2)$ in space, we try to also achieve a higher order in time, $\mathcal{O}(\tau^2)$, while not enlarging the stencil. To do so, we recast (3a) as

$$\frac{u(x_i, t^{p+1}) - u(x_i, t^p)}{\tau} - \frac{\tau}{2}\frac{\partial^2 u}{\partial t^2}(x_i, t^p) = \frac{\partial u}{\partial t}(x_i, t^p) + \mathcal{O}(\tau^2). \tag{4}$$

Hence, if the derivative $\frac{\partial^2 u}{\partial t^2}(x_i, t^p)$ is known, we can increase the order from $\mathcal{O}(\tau)$ to $\mathcal{O}(\tau^2)$ on the same stencil. The second derivative with respect to time can be obtained by differentiating the original equation (1):

$$\frac{\partial^2 u}{\partial t^2} = \frac{\partial f}{\partial t} - \frac{\partial f}{\partial x} + \frac{\partial^2 u}{\partial x^2}. \tag{5}$$

Consequently, (4) becomes:

$$\frac{u(x_i, t^{p+1}) - u(x_i, t^p)}{\tau} - \frac{\tau}{2}\frac{\partial^2 u}{\partial x^2}(x_i, t^p) - \frac{\tau}{2}\left[\frac{\partial f}{\partial t} - \frac{\partial f}{\partial x}\right] = \frac{\partial u}{\partial t}(x_i, t^p) + \mathcal{O}(\tau^2). \tag{6}$$

The next consideration is to realize that the second derivative with respect to x in (6) does not need to be known precisely. One can approximate it with sufficient accuracy. Employing the conventional central difference in space, we transform (6) into

$$\frac{u(x_i, t^{p+1}) - u(x_i, t^p)}{\tau} - \frac{\tau}{2}\frac{u(x_{i+1}, t^p) - 2u(x_i, t^p) + u(x_{i-1}, t^p)}{h^2}$$
$$- \frac{\tau}{2}\left[\frac{\partial f}{\partial t}(x_i, t^p) - \frac{\partial f}{\partial x}(x_i, t^p)\right] = \frac{\partial u}{\partial t}(x_i, t^p) + \mathcal{O}(\tau^2 + \tau h^2). \tag{7}$$

Finally, taking the approximate expression for $\frac{\partial u}{\partial t}$ from (7) and the approximate expression for $\frac{\partial u}{\partial x}$ from (3b) and substituting into (1), we arrive at the following scheme instead of (2):

$$\frac{u_i^{p+1} - u_i^p}{\tau} + \frac{u_{i+1}^p - u_{i-1}^p}{2h} - \frac{\tau}{2}\frac{u_{i+1}^p - 2u_i^p + u_{i-1}^p}{h^2} = f_i^p + \frac{\tau}{2}\left[\frac{\partial f}{\partial t} - \frac{\partial f}{\partial x}\right]_i^p. \tag{8}$$

Equation (8) is the Lax-Wendroff scheme for the differential equation (1). It is consistent with order $\mathcal{O}(\tau^2 + h^2 + \tau h^2)$ but only on the solutions of (1) rather than on all sufficiently smooth functions, since in the course of derivation we have used the equation-based differentiation (5). Accordingly, replacing the second derivative with respect to x in (6) by the central difference in (7) is referred to as equation-based differencing.

Scheme (8) employs the same four-node stencil operating on the solution u as scheme (2) does: $\{(i+1, p), (i, p), (i-1, p), (i, p+1)\}$. Yet scheme (8) is consistent with order $\mathcal{O}(\tau^2 + h^2 + \tau h^2)$ whereas scheme (2) is consistent only with a lower order $\mathcal{O}(\tau + h^2)$. The trade-off is in the structure of the approximating space—it is narrower for scheme (8) (solutions only) and wider for scheme (2) (all sufficiently smooth functions). The reduction of the approximating space for scheme (8) does not present any loss of generality. Indeed, according to the Lax theorem if the scheme is consistent *on the solutions of the original differential equation* and stable, then it is convergent. It is well-known that scheme (8) is stable if and only if $\tau/h \leq 1$. Consequently, it is convergent and offers the overall accuracy of $\mathcal{O}(\tau^2 + h^2)$ as long as the stability condition holds (because for $\tau \sim h$ we can write for the third term in the consistency estimate: $\tau h^2 \sim h^3$).

It is interesting to note that scheme (2) is unstable [45, p. 354] and thus offers no accuracy at all, even though it is consistent. We see, however, that this instability presents no barrier for using scheme (2) as a departure point for deriving scheme (8), which is stable.

A distinctive feature of scheme (8) is that the right-hand side of the difference equation gets transformed. It no longer contains only the source term f of the original differential equation projected on the grid, but also contains the first derivatives $\frac{\partial f}{\partial t}$ and $\frac{\partial f}{\partial x}$ that need to be evaluated at the node (i, p). If the function $f(x, t)$ in (1) is specified by an analytical expression, then the differentiation needed for (8) can also be done analytically. Otherwise, $\frac{\partial f}{\partial t}$ and $\frac{\partial f}{\partial x}$ on the right-hand side of (8) should be approximated on the grid. In doing so, one employs a similar consideration to that used when replacing the second derivative $\frac{\partial^2 u}{\partial x^2}$ in (6) by the central difference in (7). Namely, to achieve the overall desired accuracy of $\mathcal{O}(\tau^2 + h^2)$, the derivatives $\frac{\partial f}{\partial t}$ and $\frac{\partial f}{\partial x}$ do not need to be known precisely; it is sufficient to have them approximated with at least first order accuracy. For example, to approximately differentiate the data, we can use the same four-node stencil $\{(i+1, p), (i, p), (i-1, p), (i, p+1)\}$ on the right-hand side of (8) as we use on its right-hand side, which yields:

$$\left[\frac{\partial f}{\partial t} - \frac{\partial f}{\partial x}\right]_i^p = \frac{f_i^{p+1} - f_i^p}{\tau} - \frac{f_{i+1}^p - f_{i-1}^p}{2h} + \mathcal{O}\big(\tau + h^2\big).$$

We therefore conclude that in the general case, when we are not assuming that the data are available analytically, scheme (8) needs to employ two stencils—one for the left-hand side of the equation and the other for its right-hand side.

An important advantage of the second order scheme (8) over the leap-frog scheme, which is also second order accurate, but requires a larger stencil in the t direction, is that scheme (8) needs one initial condition, i.e., exactly as many as the differential equation (1) does, whereas the leap-frog scheme needs an additional initial condition, see, e.g., [45, p. 329].

2.2 Compact High Order Scheme for the Variable Coefficient Helmholtz Equation

For the Helmholtz equation with a variable wavenumber

$$\frac{\partial^2 u}{\partial x^2} + \frac{\partial^2 u}{\partial y^2} + k^2(x, y)u = f(x, y) \tag{9}$$

we introduce a uniform in each direction Cartesian grid with the sizes h_x and h_y. Then, using the same idea as outlined in Sect. 2.1, we obtain the equation-based compact scheme:

$$\begin{aligned}
&\frac{u_{i+1,j}-2u_{i,j}+u_{i-1,j}}{h_x^2}+\frac{u_{i,j+1}-2u_{i,j}+u_{i,j-1}}{h_y^2}+\left(k^2u\right)_{i,j}\\
&\quad+\left(\frac{h_x^2}{12}+\frac{h_y^2}{12}\right)\frac{1}{h_x^2}\left(\frac{u_{i+1,j+1}-2u_{i+1,j}+u_{i+1,j-1}}{h_y^2}\right.\\
&\quad\left.-2\frac{u_{i,j+1}-2u_{i,j}+u_{i,j-1}}{h_y^2}+\frac{u_{i-1,j+1}-2u_{i-1,j}+u_{i-1,j-1}}{h_y^2}\right)\\
&\quad+\frac{h_x^2}{12}\frac{(k^2u)_{i+1,j}-2(k^2u)_{i,j}+(k^2u)_{i-1,j}}{h_x^2}+\frac{h_y^2}{12}\frac{(k^2u)_{i,j+1}-2(k^2u)_{i,j}+(k^2u)_{i,j-1}}{h_y^2}\\
&=\frac{h_x^2}{12}\frac{f_{i+1,j}-2f_{i,j}+f_{i-1,j}}{h_x^2}+\frac{h_y^2}{12}\frac{f_{i,j+1}-2f_{i,j}+f_{i,j-1}}{h_y^2}+f_{i,j}. \qquad (10)
\end{aligned}$$

Details of the derivation and accuracy analysis of scheme (10) can be found in [20, 47]. The scheme provides *fourth order accuracy on smooth solutions of* (9).

Scheme (10) employs two stencils. The nine-node 3×3 stencil $\{(i,j),(i\pm1,j),(i,j\pm1),(i\pm1,j\pm1)\}$ is used for the discrete solution $u_{i,j}$, and the five-node stencil $\{(i,j),(i\pm1,j),(i,j\pm1)\}$ is used for the source function $f_{i,j}$, see Fig. 1. Since the left-hand side stencil is 3×3, the resulting difference equation with respect to the unknown grid function $u_{i,j}$ is second order. Therefore, the compact scheme (10) does not require additional boundary conditions beyond those needed for the original differential equation (9) itself. Neumann boundary conditions can also be included without expanding the stencil [47].

In [5], we constructed a similar compact fourth order scheme for the standard Helmholtz equation, but in polar coordinates, which entails variable coefficients. In [6], we have extended the analysis to the case of a more general Helmholtz equation, with variable coefficients under the derivatives in the Laplacian-like part.

Extension of scheme (10) to three space dimensions is straightforward, see [6]. In 3D, the scheme will employ a $3\times3\times3$ stencil on the left-hand side and a seven-node central difference stencil on the right-hand side.

Moreover, even higher accuracy can be achieved using the same compact stencils as shown in Fig. 1. Singer and Turkel [48] have constructed a sixth order accurate equation-based scheme for the constant coefficient Helmholtz equation. An extension to variable wavenumbers k has been constructed as well, and will be reported in a future publication. Similar sixth order accurate schemes, for constant coefficients, are discussed in [31, 51].

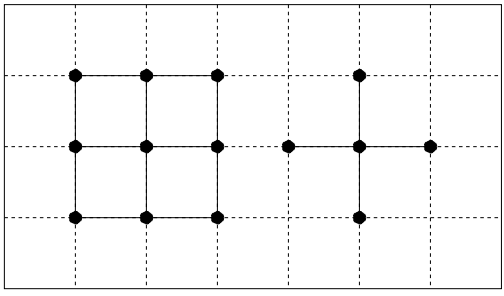

Fig. 1 Stencils of the compact scheme (10). The nine-node 3×3 stencil operating on the solution is on the *left*, and the five-node stencil operating on the data is on the *right*

A number of alternative approaches (not necessarily equation-based in the foregoing sense) have been proposed for the construction of compact high order accurate schemes, see, e.g., [28, 53].

3 Difference Potentials and Projections

3.1 Continuous Calderon's Operators

3.1.1 Constant Coefficients

We now illustrate the key concepts of the method with a simple example. We later extend this to more complicated cases. Let $\boldsymbol{L}u = 0$ be a constant coefficient second order PDE on the domain $\Omega \subset \mathbb{R}^n$ with boundary $\Gamma = \partial\Omega$. For example, it can be the Helmholtz equation (9) with $a \equiv b \equiv 1$ and $k = \text{const}$ on $\Omega \subset \mathbb{R}^2$. Let $G = G(\boldsymbol{x} - \boldsymbol{y})$ be the fundamental solution of $\boldsymbol{L}$. Then, the solution $u(\boldsymbol{x})$ on the domain Ω is given by Green's formula:

$$u(\boldsymbol{x}) = \int_\Gamma \left(u(\boldsymbol{y}) \frac{\partial G}{\partial n}(\boldsymbol{x} - \boldsymbol{y}) - \frac{\partial u}{\partial n}(\boldsymbol{y}) G(\boldsymbol{x} - \boldsymbol{y}) \right) ds_y, \quad \boldsymbol{x} \in \Omega. \tag{11}$$

A generalized potential of Calderon type [41, 42] with vector density $\boldsymbol{\xi}_\Gamma = (\xi_0, \xi_1)|_\Gamma$ is defined by the same convolution integral as on the right-hand side of (11):

$$\boldsymbol{P}_\Omega \boldsymbol{\xi}_\Gamma(\boldsymbol{x}) = \int_\Gamma \left(\xi_0(\boldsymbol{y}) \frac{\partial G}{\partial n}(\boldsymbol{x} - \boldsymbol{y}) - \xi_1(\boldsymbol{y}) G(\boldsymbol{x} - \boldsymbol{y}) \right) ds_y, \quad \boldsymbol{x} \in \Omega. \tag{12}$$

For any $\boldsymbol{\xi}_\Gamma$ we have $\boldsymbol{L}[\boldsymbol{P}_\Omega \boldsymbol{\xi}_\Gamma(\boldsymbol{x})] = 0$ on Ω. However, in general the Dirichlet data of $\boldsymbol{P}_\Omega \boldsymbol{\xi}_\Gamma$ on Γ will not coincide with ξ_0 and the Neumann data will not coincide with ξ_1. However, if the density $\boldsymbol{\xi}_\Gamma$ happens to be the trace on Γ of an actual solution u in the sense

$$\boldsymbol{\xi}_\Gamma = \boldsymbol{Tr}\, u \stackrel{\text{def}}{=} \left(u, \frac{\partial u}{\partial n} \right) \Big|_\Gamma, \tag{13}$$

then $\boldsymbol{P}_\Omega \boldsymbol{\xi}_\Gamma(\boldsymbol{x}) = u(\boldsymbol{x})$ for $\boldsymbol{x} \in \Omega$, and (12) becomes the classical Green's formula (11).

The Calderon projection $\boldsymbol{P}_\Gamma$ is the trace on Γ of the potential $\boldsymbol{P}_\Omega$ of (12):

$$\boldsymbol{P}_\Gamma \boldsymbol{\xi}_\Gamma \stackrel{\text{def}}{=} \boldsymbol{Tr}\, \boldsymbol{P}_\Omega \boldsymbol{\xi}_\Gamma. \tag{14}$$

The operator $\boldsymbol{P}_\Gamma$ of (14) is indeed a projection. To show that, we take an arbitrary function $\boldsymbol{\xi}_\Gamma$ and denote the potential by $v(\boldsymbol{x}) = \boldsymbol{P}_\Omega \boldsymbol{\xi}_\Gamma, \boldsymbol{x} \in \Omega$. Then, $\boldsymbol{L}v = 0$ and hence we can apply Green's formula (11) to the function v writing it in the form

$$v(\boldsymbol{x}) = \boldsymbol{P}_\Omega\, \boldsymbol{Tr}\, v, \quad \boldsymbol{x} \in \Omega, \tag{15}$$

where the operator $\boldsymbol{Tr}$ is defined by formula (13). Replacing v by $\boldsymbol{P}_\Omega \boldsymbol{\xi}_\Gamma$ on both sides of (15) we have: $\boldsymbol{P}_\Omega \boldsymbol{\xi}_\Gamma = \boldsymbol{P}_\Omega\, \boldsymbol{Tr}\, \boldsymbol{P}_\Omega \boldsymbol{\xi}_\Gamma$. Taking the trace of both sides yields $\boldsymbol{P}_\Gamma \boldsymbol{\xi}_\Gamma = \boldsymbol{P}_\Gamma^2 \boldsymbol{\xi}_\Gamma$.

The key property of the projection operator $\boldsymbol{P}_\Gamma$ in (14) is the following (see [30, 41, 42]).

Theorem 1 *A given boundary function $\boldsymbol{\xi}_\Gamma$ is the trace of a solution $u(\boldsymbol{x})$ to the homogeneous equation $\boldsymbol{L}u = 0$ on Ω: $\boldsymbol{\xi}_\Gamma = \boldsymbol{Tr}\, u$, if and only if it satisfies the boundary equation with projection (BEP):*

$$\boldsymbol{P}_\Gamma \boldsymbol{\xi}_\Gamma = \boldsymbol{\xi}_\Gamma. \tag{16}$$

Proof Let $u(\boldsymbol{x})$ be a sufficiently smooth solution of equation $\boldsymbol{L}u = 0$ on the domain Ω, and let $\boldsymbol{\xi} = \boldsymbol{Tr}\, u$. Then, applying the operator $\boldsymbol{Tr}$ of (13) to Green's formula (15) written for u:

$$u(\boldsymbol{x}) = \boldsymbol{P}_\Omega\, \boldsymbol{Tr}\, u, \quad \boldsymbol{x} \in \Omega,$$

we obtain the BEP (16). Conversely, let equality (16) hold for some $\boldsymbol{\xi}_\Gamma$. Denote

$$u = \boldsymbol{P}_\Omega \boldsymbol{\xi}_\Gamma,$$

then $\boldsymbol{L}u = 0$ on Ω. In addition, equality (16) implies that $\boldsymbol{Tr}\, u = \boldsymbol{\xi}_\Gamma$. Thus, we have obtained the required solution u on Ω, for which $\boldsymbol{\xi}_\Gamma$ is the trace. This proof originally comes from [41]. □

Next, assume that $\boldsymbol{\xi}_\Gamma = (\xi_0, \xi_1)$ is given, and take an arbitrary sufficiently smooth and compactly supported function $w(\boldsymbol{x})$, $\boldsymbol{x} \in \mathbb{R}^n$, that satisfies $\boldsymbol{Tr}\, w = \boldsymbol{\xi}_\Gamma$. (We shall see that for the discrete case finding an appropriate counterpart of w is trivial.) Since, in general $\boldsymbol{L}w \neq 0$, $\boldsymbol{x} \in \Omega$, Green's formula for w becomes [cf. formula (11)]:

$$w(\boldsymbol{x}) = \int_\Omega G\boldsymbol{L}w d\boldsymbol{y} + \int_\Gamma \left(w\frac{\partial G}{\partial n} - \frac{\partial w}{\partial n} G \right) ds_y, \quad \boldsymbol{x} \in \Omega.$$

We recast this as:

$$w(\boldsymbol{x}) - \int_\Omega G\boldsymbol{L}w d\boldsymbol{y} = \int_\Gamma \left(w\frac{\partial G}{\partial n} - \frac{\partial w}{\partial n} G \right) ds_y, \quad \boldsymbol{x} \in \Omega.$$

Note that the right-hand side of this equation coincides with the right-hand side of (12) because $\boldsymbol{Tr}\, w = \boldsymbol{\xi}_\Gamma$. Therefore, the Calderon potential (12) can be equivalently re-defined as:

$$\boldsymbol{P}_\Omega \boldsymbol{\xi}_\Gamma(\boldsymbol{x}) = w(\boldsymbol{x}) - \int_\Omega G\boldsymbol{L}w d\boldsymbol{y}, \quad \boldsymbol{x} \in \Omega. \tag{17}$$

It is clear that the potential (17) is insensitive to the choice of $w(\boldsymbol{x})$ as long as $\boldsymbol{Tr}\, w = \boldsymbol{\xi}_\Gamma$. The projection $\boldsymbol{Tr}\, \boldsymbol{P}_\Omega$ defined via formula (17) is the same as $\boldsymbol{P}_\Gamma$ of (14). However, the new definition (17) does not contain surface integrals and allows us to define Calderon's operators for the case of variable coefficients, when there is no known fundamental solution, see Sect. 3.1.2.

If the governing equation is inhomogeneous on Ω: $\boldsymbol{L}u = f$, then the BEP (16) transforms into (see [41, 42])

$$\boldsymbol{P}_\Gamma \boldsymbol{\xi}_\Gamma + \boldsymbol{Tr}\, \boldsymbol{G} f = \boldsymbol{\xi}_\Gamma, \tag{18}$$

where $\boldsymbol{G}$ denotes the Green's operator, i.e., the inverse: $\boldsymbol{G}f = \int_\Omega G(\boldsymbol{x} - \boldsymbol{y}) f(\boldsymbol{y}) d\boldsymbol{y}$. Theorem 1 also gets modified accordingly: a given $\boldsymbol{\xi}_\Gamma$ satisfies the inhomogeneous BEP (18) if and only if it is the trace of a solution $u(\boldsymbol{x})$ to the inhomogeneous equation $\boldsymbol{L}u = f$ on the domain Ω. The proof of this equivalence statement is very similar to the proof of Theorem 1.

3.1.2 Variable Coefficients

We denote

$$g(\boldsymbol{x}) = \begin{cases} \boldsymbol{L}w, & \boldsymbol{x} \in \Omega, \\ 0, & \boldsymbol{x} \notin \Omega. \end{cases} \tag{19}$$

Then, the volume convolution integral on the right-hand side of formula (17) is a solution to the equation $\boldsymbol{L}v = g$. This solution is obtained on $\mathbb{R}^n$ and then restricted to Ω. Using the Green's operator notation [introduced right after equation (18)] we can rewrite formula (17) as:

$$\boldsymbol{P}_{\Omega}\boldsymbol{\xi}_{\Gamma} = w - \boldsymbol{G}g \equiv w - \boldsymbol{G}(\boldsymbol{L}w|_{\Omega}), \quad \boldsymbol{x} \in \Omega. \tag{20}$$

Now, let $\boldsymbol{L}$ be a more general operator, e.g., the variable coefficient Helmholtz operator of (9), and let Ω_0 be a larger region, $\Omega \subset \Omega_0 \subseteq \mathbb{R}^n$. Assume that for any sufficiently smooth function g the equation $\boldsymbol{L}v = g$ has a unique solution on Ω_0 that satisfies the given boundary condition on $\partial\Omega_0$.

Definition 1 The problem of solving equation $\boldsymbol{L}v = g$ on Ω_0 subject to the chosen boundary condition on $\partial\Omega_0$ is referred to as the *auxiliary problem* (AP). We denote its solution operator, i.e., the inverse operator for $\boldsymbol{L}$ subject to a given boundary condition on $\partial\Omega_0$, by $\boldsymbol{G}$, so that $v = \boldsymbol{G}g$.

With the new, more general, operators $\boldsymbol{L}$ and $\boldsymbol{G}$, formula (20) still defines a generalized Calderon's potential, and the operator $\boldsymbol{P}_{\Gamma} = \boldsymbol{Tr}\,\boldsymbol{P}_{\Omega}$ is still a projection, i.e., $\boldsymbol{P}_{\Gamma}^2 = \boldsymbol{P}_{\Gamma}$. The key property of the new projection $\boldsymbol{P}_{\Gamma}$ is the same as that given by Theorem 1:

$$\boldsymbol{P}_{\Gamma}\boldsymbol{\xi}_{\Gamma} = \boldsymbol{\xi}_{\Gamma} \quad \Leftrightarrow \quad \exists u : \boldsymbol{\xi}_{\Gamma} = \boldsymbol{Tr}\,u \;\&\; \boldsymbol{L}u = 0 \quad \text{on } \Omega. \tag{21}$$

In other words, a given density $\boldsymbol{\xi}_{\Gamma}$ belongs to the range of the projection, $\boldsymbol{\xi}_{\Gamma} \in \mathrm{Im}\boldsymbol{P}_{\Gamma}$, iff it is the trace of a solution to $\boldsymbol{L}u = 0$ on Ω. The proof of this result uses the notion of clear or minimal trace (or, alternatively, the notion of generalized potential with the density from the space of jumps), and can be found in [42, Part II, Chap. 1]. We note that for the equation with variable coefficients (9) and $a(x, y) \neq b(x, y)$ it may be more natural and more beneficial, although not necessary, to redefine the functions $\boldsymbol{\xi}_{\Gamma}$ and the operator $\boldsymbol{Tr}$, see formula (13), and instead of the standard normal derivative $\frac{\partial u}{\partial n}$ use the co-normal derivative $a\frac{\partial u}{\partial x}n_x + b\frac{\partial u}{\partial y}n_y$.

We emphasize that the projection $\boldsymbol{P}_{\Gamma}$ can be built using different APs. If the AP changes, so does the operator $\boldsymbol{G}$ and hence $\boldsymbol{P}_{\Gamma}$, but the range of the projection $\mathrm{Im}\boldsymbol{P}_{\Gamma}$ remains unaffected, because it contains traces of the solutions and only those traces. In other words, when changing the AP one changes the projection angle onto the same subspace [42].

The flexibility in choosing the AP of Definition 1 translates into the flexibility of computing $\boldsymbol{G}$ and hence $\boldsymbol{P}_{\Gamma}$. We choose the domain Ω_0 and the boundary condition at $\partial\Omega_0$ so that the AP be computationally easy to solve. In most cases, the solver will not involve convolutions. For constant coefficients, it may be based on a FFT. For variable coefficients, it may be either a direct or an iterative solver. Our choices for the current study are outlined in Sect. 5.

If the governing equation with variable coefficients is inhomogeneous on Ω, $\boldsymbol{L}u = f$, then instead of the homogeneous BEP of (21) the solutions u are characterized by the inhomogeneous BEP:

$$\boldsymbol{P}_{\Gamma}\boldsymbol{\xi}_{\Gamma} + \boldsymbol{Tr}\,\boldsymbol{G}f = \boldsymbol{\xi}_{\Gamma}, \tag{22a}$$

where $\boldsymbol{G}$ is the solution operator for the AP. Equation (22a) holds for a given $\boldsymbol{\xi}_{\Gamma}$ if and only if

$$\exists u : \boldsymbol{\xi}_{\Gamma} = \boldsymbol{Tr}\,u \;\&\; \boldsymbol{L}u = f \quad \text{on } \Omega. \tag{22b}$$

The equivalence of (22a) and (22b) implies that the differential equation $\boldsymbol{L}u = f$, with the entire variety of its solutions, is reduced from the domain Ω to the boundary Γ. In other words, those and only those functions u on Ω that solve $\boldsymbol{L}u = f$ have traces $\boldsymbol{\xi}_\Gamma$ that solve $\boldsymbol{P}_\Gamma \boldsymbol{\xi}_\Gamma + \boldsymbol{Tr}\,\boldsymbol{G} f = \boldsymbol{\xi}_\Gamma$. This is a far more general result than that of the classical potential theory, when specific boundary value problems, such as Dirichlet or Neumann, are reduced to Fredholm integral equations using specific representations, a double-layer or a single-layer potential with an auxiliary density, respectively.

3.1.3 Boundary Conditions

Once the BEP of (22a), (22b) holds for some $\boldsymbol{\xi}_\Gamma$, the corresponding solution $u(\boldsymbol{x})$ on Ω is given by the generalized Green's formula:

$$u = \boldsymbol{P}_\Omega \boldsymbol{\xi}_\Gamma + \boldsymbol{G} f. \tag{23}$$

However, the BEP $\boldsymbol{P}_\Gamma \boldsymbol{\xi}_\Gamma + \boldsymbol{Tr}\,\boldsymbol{G} f = \boldsymbol{\xi}_\Gamma$ itself has multiple solutions $\boldsymbol{\xi}_\Gamma$ on Γ, because the equation $\boldsymbol{L}u = f$ has multiple solutions u on Ω. To obtain a unique solution, one must impose boundary conditions on u, i.e., formulate a boundary value problem:

$$\boldsymbol{L}u = f \quad \text{on } \Omega \quad \text{and} \quad \boldsymbol{l}_\Gamma u = \phi \quad \text{on } \Gamma. \tag{24}$$

Then, the boundary condition $\boldsymbol{l}_\Gamma u = \phi$ of (24) can be recast as

$$\boldsymbol{l}_\Gamma(\boldsymbol{P}_\Omega \boldsymbol{\xi}_\Gamma + \boldsymbol{G} f) = \phi, \tag{25}$$

and the system of (22a), (25) is solved with respect to $\boldsymbol{\xi}_\Gamma$. In doing so, the operator $\boldsymbol{l}_\Gamma$ that defines the boundary condition in problem (24) can be arbitrary, ranging from very simple (e.g., Dirichlet or Neumann) to very general (e.g., different type on different parts of Γ, nonlocal, etc.), yet system (22a), (25) on Γ is still equivalent to problem (24).

We emphasize that whereas system (22a), (25) automatically allows for variable coefficients inside Ω and basically any boundary condition on Γ, the classical potential theory is limited to constant coefficients, and finding an appropriate boundary representation that would lead to a Fredholm equation of the second kind requires special effort on a case-by-case basis as soon as the boundary condition starts to differ from the simplest Dirichlet or Neumann type.

3.1.4 Well-Posedness

We assume that the original boundary value problem (24) is well-posed, i.e., that its solution exists, is unique, and continuously depends on the data f, ϕ in the sense of appropriately chosen norms. Then, the equivalent problem on the boundary (18), (25) is also well-posed. This means that if the BEP is perturbed, then the solution of the boundary system will also get perturbed, and the perturbation of the solution will be bounded in the appropriate norm by the perturbation introduced into the BEP.

Specifically, consider the homogeneous case:

$$\boldsymbol{L}u = 0 \quad \text{on } \Omega \quad \text{and} \quad \boldsymbol{l}_\Gamma u = \phi \quad \text{on } \Gamma,$$

for which the equivalent boundary formulation is

$$\boldsymbol{P}_\Gamma \boldsymbol{\xi}_\Gamma - \boldsymbol{\xi}_\Gamma = \boldsymbol{0} \quad \text{and} \quad \boldsymbol{l}_\Gamma(\boldsymbol{P}_\Omega \boldsymbol{\xi}_\Gamma) = \phi. \tag{26}$$

If the original problem is well-posed, then $\|u\|_\Omega \le c\|\phi\|_\Gamma$, and consequently,

$$\|\boldsymbol{\xi}_\Gamma\|'_\Gamma \le c_1\|\phi\|_\Gamma. \tag{27}$$

This result has nothing to do with Calderon operators per se, it holds simply because $\boldsymbol{\xi}_\Gamma = \boldsymbol{Tr}\, u$. The choice of the norms $\|\cdot\|_\Omega$, $\|\cdot\|_\Gamma$, and $\|\cdot\|'_\Gamma$ is discussed in [42, Part I]; for example, one can use the classical Hölder norms that account for the proper relationships between the regularity of the solution u on the domain Ω, the boundary data ϕ, and the boundary trace $\boldsymbol{\xi}_\Gamma$.

Let us now assume that the BEP (16), which is equivalent to $\boldsymbol{L}u = 0$ on Ω, is not enforced exactly, so that there is a perturbation $\boldsymbol{\psi}_\Gamma$ on the right-hand side, and instead of the original problem (26) we are solving

$$\boldsymbol{P}_\Gamma\boldsymbol{\xi}_\Gamma - \boldsymbol{\xi}_\Gamma = \boldsymbol{\psi}_\Gamma \quad \text{and} \quad \boldsymbol{l}_\Gamma(\boldsymbol{P}_\Omega\boldsymbol{\xi}_\Gamma) = \phi. \tag{28}$$

In practice, the perturbation $\boldsymbol{\psi}_\Gamma$ can be associated with the perturbations of the data (inhomogeneity of the differential equation), or those of the coefficients of $\boldsymbol{L}$, but its precise nature is not important. We interpret $\boldsymbol{\psi}_\Gamma$ in formula (28) as a generic perturbation of the BEP; and by definition, $\boldsymbol{\psi}_\Gamma$ belongs to the same space as $\boldsymbol{\xi}_\Gamma$ does. Then, estimate (27) generalizes to

$$\|\boldsymbol{\xi}_\Gamma\|'_\Gamma \le C\big(\|\phi\|_\Gamma + \|\boldsymbol{\psi}_\Gamma\|'_\Gamma\big),$$

where *the constant C depends on the induced operator norms $\|\boldsymbol{P}_\Omega\|$ and $\|\boldsymbol{P}_\Gamma\|$, but does not depend on either ϕ or $\boldsymbol{\psi}_\Gamma$*. The proof can be found in [42, Part II, Chap. 1]. It is based on splitting the entire space of traces $\boldsymbol{\xi}_\Gamma$ on Γ into the direct sum: $\mathrm{Im}\boldsymbol{P}_\Gamma \oplus \mathrm{Ker}\boldsymbol{P}_\Gamma$. For wave propagation problems, this implies the split into the subspaces of incoming and outgoing waves with respect to Ω [30].

Unlike the method of difference potentials, BEM does not guarantee the well posedness automatically, and one always needs to make sure that the boundary representation is given by Fredholm integral equations of the second kind, see, e.g., [40], which may not be an easy task for general boundary conditions.

3.2 Difference Potentials and Projections

We now define the difference potentials and discrete boundary projections for compact schemes and describe their key properties. The corresponding definitions require additional constructs compared to those given in [42] for standard schemes.

Let $\Omega_0 \supset \Omega$ be a regular domain, e.g., a rectangle in 2D or a parallelepiped in 3D, and let $\mathbb{N}_0$, $\mathbb{M}_0$, and $\mathbb{K}_0$ be three discretizations grids on Ω_0. Those grids may fully or partially coincide (see Fig. 2), although in general they do not have to. For efficiency and convenience, one should choose regular, e.g. Cartesian or polar, grids.

We approximate the solution u and the right-hand side f of the differential equation $\boldsymbol{L}u = f$ on the grids $\mathbb{N}_0$ and $\mathbb{K}_0$, respectively. To distinguish between continuous functions of the argument $\boldsymbol{x}$ and discrete functions on the grid, we will use the notations $\mathfrak{u}$, $\mathfrak{f}$, etc., for the latter. Let $\mathfrak{U}_0$ be the space of grid functions defined on $\mathbb{N}_0$ and let $\mathfrak{F}_0$ be the space of grid functions on $\mathbb{K}_0$. Then, for the discrete solution $\mathfrak{u}$ we have $\mathfrak{u} \in \mathfrak{U}_0$, and for the discrete source function $\mathfrak{f}$ we have $\mathfrak{f} \in \mathfrak{F}_0$.

On the grid $\mathbb{M}_0$ we define the residuals of the difference operators we use to construct the approximation. Let $\mathfrak{G}_0$ be the space of grid functions defined on $\mathbb{M}_0$. Then, we introduce

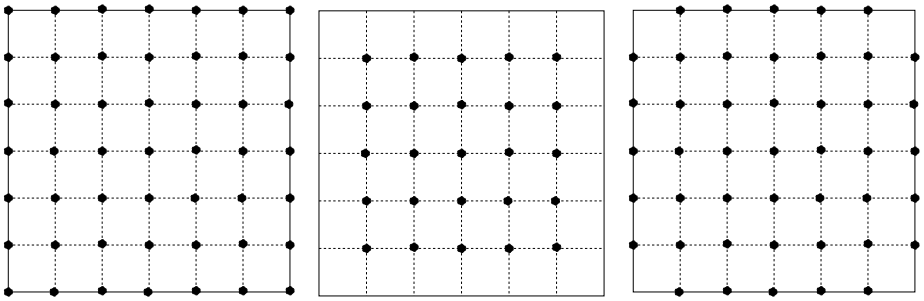

Fig. 2 Cartesian grids for the compact scheme (10)

two operators:

$$\boldsymbol{L}^{(h)} : \mathfrak{U}_0 \mapsto \mathfrak{G}_0 \quad \text{and} \quad \boldsymbol{B}^{(h)} : \mathfrak{F}_0 \mapsto \mathfrak{G}_0.$$

The operator $\boldsymbol{L}^{(h)}$ applies to the discrete solution $\mathfrak{u}$, and the operator $\boldsymbol{B}^{(h)}$ applies to the data $\mathfrak{f}$. The compact approximation can therefore be symbolically written as

$$\boldsymbol{L}^{(h)}\mathfrak{u} = \boldsymbol{B}^{(h)}\mathfrak{f}, \tag{29}$$

where $\mathfrak{u}$ and $\mathfrak{f}$ are defined on the grids $\mathbb{N}_0$ and $\mathbb{K}_0$, respectively, whereas equality (29) itself is enforced at the nodes of the grid $\mathbb{M}_0$. For a given node $m \in \mathbb{M}_0$, we will hereafter denote the corresponding stencils of the operators $\boldsymbol{L}^{(h)}$ and $\boldsymbol{B}^{(h)}$ by $\mathbb{N}_m$ and $\mathbb{K}_m$, respectively.

For the compact fourth order accurate scheme (10) described in Sect. 2.2, $\mathbb{N}_m$ is a nine-node 3×3 stencil and $\mathbb{K}_m$ a five-node central difference stencil. They are depicted in Fig. 1 (on the left and on the right, respectively). The corresponding grids $\mathbb{N}_0$, $\mathbb{M}_0$, and $\mathbb{K}_0$ for a square domain Ω_0 are schematically shown in Fig. 2. According to the structure of the stencils $\mathbb{N}_m$ and $\mathbb{K}_m$, the grid $\mathbb{N}_0$ consists of all Cartesian nodes on the square (see Fig. 2(a)), the grid $\mathbb{M}_0$ consists of all the nodes except the outermost nodes (see Fig. 2(b)), and the grid $\mathbb{K}_0$ consists of all the nodes except the four corner nodes (see Fig. 2(c)). The corner nodes are excluded from $\mathbb{K}_0$ because in order to obtain $\boldsymbol{B}^{(h)}\mathfrak{f}$ on $\mathbb{M}_0$, one does not need to know $\mathfrak{f}$ at the corners. (Note, in 3D both corner nodes and edge nodes would be excluded from $\mathbb{K}_0$.)

We now supplement the definition of the space $\mathfrak{U}_0$ by boundary conditions on the boundary of the square Ω_0. We require that these boundary conditions be such as to guarantee that the discrete equation $\boldsymbol{L}^{(h)}\mathfrak{u} = \mathfrak{g}$ has a unique solution $\mathfrak{u} \in \mathfrak{U}_0$ for any arbitrary $\mathfrak{g} \in \mathfrak{G}_0$, i.e., for any grid function $\mathfrak{g}$ specified on $\mathbb{M}_0$. Note that since the scheme we are using is compact, the discrete equation does not require any additional boundary conditions at $\partial\Omega_0$ beyond what is needed for the original differential equation.

Definition 2 The problem

$$\boldsymbol{L}^{(h)}\mathfrak{u} = \mathfrak{g}, \quad \mathfrak{u} \in \mathfrak{U}_0, \tag{30}$$

will be referred to as the *discrete auxiliary problem* (cf. continuous Definition 1 in Sect. 3.1.2).

Solution of the discrete AP (30) defines the discrete Green's operator:

$$\boldsymbol{G}^{(h)} : \mathfrak{G}_0 \mapsto \mathfrak{U}_0,$$

i.e., the inverse operator to $\boldsymbol{L}^{(h)}$ under the constraint $\mathfrak{u} \in \mathfrak{U}_0$. Note that while the choice of the boundary condition for the discrete AP, i.e., the definition of the space $\mathfrak{U}_0$, affects the operator $\boldsymbol{G}^{(h)}$ and hence the discrete potentials and projections that we introduce below, it does not affect the final approximate solution of problem (24) as long as the AP is uniquely solvable and well-posed. Therefore, it is beneficial to formulate the discrete AP so as to facilitate the most efficient numerical computation of its solution on the grid $\mathbb{N}_0$. Specific choices of the boundary conditions for the discrete AP that we made for our simulations are outlined in Sect. 5.

Note, that if the continuous source function $f(x, y)$ is sufficiently smooth on the entire square Ω_0, and if $\mathfrak{f}$ is the trace of this function on the grid $\mathbb{K}_0$, then $\mathfrak{u} = \boldsymbol{G}^{(h)}\boldsymbol{B}^{(h)}\mathfrak{f}$ is a fourth order accurate approximation of the solution u to the differential equation $\boldsymbol{L}u = f$ on Ω_0 subject to the chosen boundary condition at $\partial\Omega_0$. We, however, will also be solving the discrete AP (30) for other types of data $\mathfrak{g} \in \mathfrak{G}_0$, in particular, for data that are not necessarily regular and are not necessarily representable in the form $\boldsymbol{B}^{(h)}\mathfrak{f}$ for a smooth $\mathfrak{f}$ (i.e., smooth f).

These constructs simplify in the case of conventional, i.e., non-compact schemes. Since there is no stencil operating on the data, the operator $\boldsymbol{B}^{(h)}$ is essentially the identity. More precisely,

$$\boldsymbol{B}^{(h)}\mathfrak{f}|_m = \begin{cases} \mathfrak{f}_m, & m \in \mathbb{M}_0, \\ 0, & m \notin \mathbb{M}_0. \end{cases}$$

Consequently, the functions from $\mathfrak{F}_0$ and $\mathfrak{G}_0$ coincide on $\mathbb{M}_0$, and there is no need to keep separate grids $\mathbb{M}_0$ and $\mathbb{K}_0$ and separate spaces $\mathfrak{G}_0$ and $\mathfrak{F}_0$. Instead, the space of discrete right-hand sides $\mathfrak{F}_0$ can be defined directly on the grid $\mathbb{M}_0$, on which the residuals of the operator $\boldsymbol{L}^{(h)}$ are defined. Then, the scheme itself is written as $\boldsymbol{L}^{(h)}\mathfrak{u} = \mathfrak{f}$, where $\mathfrak{f} \in \mathfrak{F}_0$, and along with the boundary condition in the form $\mathfrak{u} \in \mathfrak{U}_0$ we obtain the discrete AP [cf. formula (30)] that should be uniquely solvable and well-posed. Previously, it was this AP that was used in the literature for constructing the difference potentials and projections for various problems, see [42] and [45, Chap. 14].

For a given domain Ω, we consider the following grid subsets:

$$\begin{aligned} &\mathbb{M}^+ = \mathbb{M}_0 \cap \Omega, \qquad \mathbb{M}^- = \mathbb{M}_0 \backslash \mathbb{M}^+ = \mathbb{M} \cap (\Omega_0 \setminus \Omega), \\ &\mathbb{N}^+ = \bigcup_{m \in \mathbb{M}^+} \mathbb{N}_m, \qquad \mathbb{N}^- = \bigcup_{m \in \mathbb{M}^-} \mathbb{N}_m, \qquad \gamma = \mathbb{N}^+ \cap \mathbb{N}^-. \end{aligned} \tag{31}$$

The set γ defined in (31) is called the *grid boundary*. It is a "fringe" of nodes of $\mathbb{N}_0$ that straddles the boundary $\Gamma = \partial\Omega$. A fragment of a grid boundary γ for the nine-node 3×3 stencil $\mathbb{N}_m$ is schematically shown in Fig. 3.

We emphasize that the partition of $\mathbb{M}_0$ into $\mathbb{M}^+$ and $\mathbb{M}^-$ defined by formula (31) is purely geometric; it is based on the location of every node of $\mathbb{M}_0$ either inside or outside Ω and so $\mathbb{M}^+ \cap \mathbb{M}^- = \emptyset$. At the same time, the sets $\mathbb{N}^+$ and $\mathbb{N}^-$ are obtained as the union of all stencils $\mathbb{N}_m$ while the center of the stencil m belongs to $\mathbb{M}^+$ and $\mathbb{M}^-$, respectively. Consequently, the sets $\mathbb{N}^+$ and $\mathbb{N}^-$ overlap, and their intersection is the grid boundary γ. We re-emphasize that the grid $\mathbb{N}_0$ is regular and is not required to conform to the shape of Γ.

Let ξ_γ be a function specified at the grid boundary γ. Choose an arbitrary $w \in \mathfrak{U}_0$ such that $w|_\gamma = \xi_\gamma$ or equivalently, $\boldsymbol{Tr}^{(h)}\, w = \xi_\gamma$. Apply the discrete operator $\boldsymbol{L}^{(h)}$ to w and truncate the result to the subset $\mathbb{M}^+ \subset \mathbb{M}_0$. The difference potential with the density ξ_γ is defined as [cf. formula (20)]:

$$\boldsymbol{P}_{\mathbb{N}^+}\xi_\gamma = w - \boldsymbol{G}^{(h)}\big(\boldsymbol{L}^{(h)}w|_{\mathbb{M}^+}\big), \quad n \in \mathbb{N}^+. \tag{32}$$

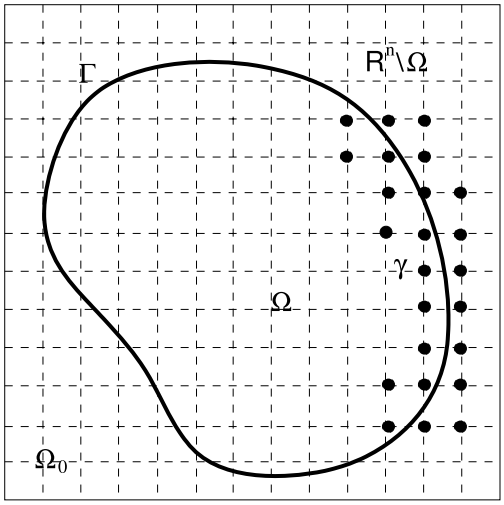

Fig. 3 Schematic for the grid boundary γ

$\boldsymbol{L}^{(h)} w|_{\mathbb{M}^+}$ means that the operator $\boldsymbol{L}^{(h)}$ is first applied to w and then the result is truncated, i.e., left unchanged on $\mathbb{M}^+$ and replaced by zero on $\mathbb{M}^- = \mathbb{M}_0 \setminus \mathbb{M}^+$. $\boldsymbol{G}^{(h)}$ in formula (32) is the inverse of $\boldsymbol{L}^{(h)}$ obtained by solving the difference AP (30) on the regular grid $\mathbb{N}_0$. By definition, the difference potential $\boldsymbol{P}_{\mathbb{N}^+}\xi_\gamma$ of (32) is a solution to the homogeneous difference equation on $\mathbb{M}^+$:

$$\boldsymbol{L}^{(h)}[\boldsymbol{P}_{\mathbb{N}^+}\xi_\gamma] = 0. \tag{33}$$

We emphasize that the right-hand side $\mathfrak{g} = \boldsymbol{L}^{(h)} w|_{\mathbb{M}^+}$, for which the discrete AP (30) is solved in order to compute the potential (32), is a special auxiliary right-hand side. We do not require that it can be represented in the form $\boldsymbol{B}^{(h)}\mathfrak{f}$, where $\mathfrak{f}$ is the trace of a smooth function $f(\boldsymbol{x})$ on the grid.

According to the definition of the difference potential (32), the difference boundary projection is given by [cf. formula (14)]:

$$\boldsymbol{P}_\gamma \xi_\gamma = \boldsymbol{Tr}^{(h)}\, \boldsymbol{P}_{\mathbb{N}^+}\xi_\gamma. \tag{34}$$

We now consider the difference equation $\boldsymbol{L}^{(h)}\mathfrak{u} = \boldsymbol{B}^{(h)}\mathfrak{f}$, see (29), but only on the sub-grid $\mathbb{M}^+$, rather then on the entire $\mathbb{M}_0$. It approximates the governing differential equation on Ω from the definition of the original boundary value problem (24). The key property of the projection $\boldsymbol{P}_\gamma$ in (34) parallels the corresponding key property in the continuous case, see (22a), (22b),—a given ξ_γ satisfies the inhomogeneous difference BEP:

$$\boldsymbol{P}_\gamma \xi_\gamma + \boldsymbol{Tr}^{(h)}\, \boldsymbol{G}^{(h)} \boldsymbol{B}^{(h)}\mathfrak{f} = \xi_\gamma \tag{35}$$

iff there exists $\mathfrak{u}$ on $\mathbb{N}^+$ such that $\boldsymbol{L}^{(h)}\mathfrak{u} = \boldsymbol{B}^{(h)}\mathfrak{f}$ on $\mathbb{M}^+$ and $\boldsymbol{Tr}^{(h)}\,\mathfrak{u} = \xi_\gamma$. If (35) holds, then the corresponding solution $\mathfrak{u}$ on $\mathbb{N}^+$ is given by the discrete generalized Green's formula [cf. formula (23)]:

$$\mathfrak{u} = \boldsymbol{P}_{\mathbb{N}^+}\xi_\gamma + \boldsymbol{G}^{(h)} \boldsymbol{B}^{(h)}\mathfrak{f}. \tag{36}$$

In other words, the discrete BEP (35) equivalently reduces the discrete approximation $\boldsymbol{L}^{(h)}\mathfrak{u} = \boldsymbol{B}^{(h)}\mathfrak{f}$ of the differential equation $\boldsymbol{L}u = f$ from the grid domain to the grid boundary γ. As in the continuous case, the discrete BEP (35) itself has multiple solutions, because

the difference equation $\boldsymbol{L}^{(h)}\mathfrak{u} = \boldsymbol{B}^{(h)}\mathfrak{f}$ has multiple solutions. To obtain a full discretization that would parallel the continuous boundary equations (22a), (25), and would have a unique solution, one also needs to take into account the boundary condition on Γ, see formula (24). This question is addressed in Sect. 4.3.

We note, that the definition of the difference potential (32) does not depend on the operator $\boldsymbol{B}^{(h)}$ that distinguishes between a compact and a conventional (i.e., non-compact) discretization. The reason for that is clear: the continuous potential (20) is a solution to the homogeneous equation $\boldsymbol{L}u = 0$ on Ω. However, when the compact scheme (29) is applied to a homogeneous equation, it becomes $\boldsymbol{L}^{(h)}\mathfrak{u} = 0$. Therefore, the operator $\boldsymbol{B}^{(h)}$ plays no role in representing the solutions to the homogeneous equations. Indeed, the difference potential (32), which is a discrete counterpart of (20), is a solution to the homogeneous equation $\boldsymbol{L}^{(h)}\mathfrak{u} = 0$ on $\mathbb{M}^+$, see formula (33).

On the other hand, for the inhomogeneous equation $\boldsymbol{L}u = f$ the contribution of the data $f(\boldsymbol{x})$ enters into the BEP (35) via $\boldsymbol{B}^{(h)}\mathfrak{f}$, where $\mathfrak{f}$ represents $f(\boldsymbol{x})$ on the grid. When computing $\boldsymbol{B}^{(h)}\mathfrak{f}$, a subtle yet important issue arises. Technically, the source function $f(\boldsymbol{x})$ in the boundary value problem (24) is given only on Ω and may not even be known/defined anywhere outside Ω. Hence, the discrete source function $\mathfrak{f}$ can be considered given only on the grid subset $\mathbb{K}_\Omega \stackrel{\text{def}}{=} (\mathbb{K}_0 \cap \Omega) \subset \mathbb{K}_0$, whereas to compute $\boldsymbol{B}^{(h)}\mathfrak{f}$ on $\mathbb{M}^+$ it needs to be known on a wider subset $\mathbb{K}^+ = \cup_{m\in\mathbb{M}^+}\mathbb{K}_m$, where $\mathbb{K}_m$ is the stencil of $\boldsymbol{B}^{(h)}$. To obtain the values of $\mathfrak{f}$ at the nodes $\mathbb{K}^+ \setminus \mathbb{K}_\Omega$ that lie outside Ω, a special extension procedure needs to be employed. This procedure, as well as other details of the computational algorithm, are discussed in Sect. 4.

4 Solution Algorithm

Hereafter, we will be computing only sufficiently smooth 2D solutions with no singularities. This implies, in particular, that all the components of the formulation that may affect the regularity of the solution, such as the source function f and the boundary data ϕ, see formula (24), have to be sufficiently smooth. The same applies not only to the data, but also to the geometry. Namely, we assume that the boundary $\Gamma = \partial\Omega$ is a smooth closed curve, see Fig. 3. The formulations that involve singular behavior, for example, due to geometric irregularities of Γ, as well as 3D formulations, will be addressed in a future publication.

4.1 Representation of the Solution at the Boundary

We begin by representing the trace of the continuous solution u to problem (24) at the boundary Γ. This will later be used to have the solution itself approximated on the grid $\mathbb{N}^+$, see (31), and reconstructed by means of the discrete Green's formula (36).

We introduce a basis in the space of functions $\boldsymbol{\xi}_\Gamma$ defined on the boundary Γ. Since $\boldsymbol{\xi}_\Gamma$ are vector-functions with two components, the basis will consist of two sets of functions:

$$\begin{aligned}&\ldots, \boldsymbol{\psi}_0^{(-j)}, \ldots, \boldsymbol{\psi}_0^{(-3)}, \boldsymbol{\psi}_0^{(-2)}, \boldsymbol{\psi}_0^{(-1)}, \boldsymbol{\psi}_0^{(0)}, \boldsymbol{\psi}_0^{(1)}, \boldsymbol{\psi}_0^{(2)}, \boldsymbol{\psi}_0^{(3)}, \ldots, \boldsymbol{\psi}_0^{(j)}, \ldots,\\ &\ldots, \boldsymbol{\psi}_1^{(-j)}, \ldots, \boldsymbol{\psi}_1^{(-3)}, \boldsymbol{\psi}_1^{(-2)}, \boldsymbol{\psi}_1^{(-1)}, \boldsymbol{\psi}_1^{(0)}, \boldsymbol{\psi}_1^{(1)}, \boldsymbol{\psi}_1^{(2)}, \boldsymbol{\psi}_1^{(3)}, \ldots, \boldsymbol{\psi}_1^{(j)}, \ldots,\end{aligned} \tag{37a}$$

where for every j

$$\boldsymbol{\psi}_0^{(j)} = \big(\psi_0^{(j)}, 0\big) \quad \text{and} \quad \boldsymbol{\psi}_1^{(j)} = \big(0, \psi_1^{(j)}\big). \tag{38}$$

So for a given $\boldsymbol{\xi}_\Gamma = (\xi_0, \xi_1)$ the expansion with respect to the basis (37a) can be written as

$$\boldsymbol{\xi}_\Gamma = \underbrace{\sum_{-\infty}^{\infty} c_{0j} \boldsymbol{\psi}_0^{(j)}}_{(\xi_0,0)} + \underbrace{\sum_{-\infty}^{\infty} c_{1j} \boldsymbol{\psi}_1^{(j)}}_{(0,\xi_1)}. \tag{37b}$$

Since Γ is a smooth closed contour, and the solutions of interest u are also smooth, we can consider *the components of* $\boldsymbol{\xi}_\Gamma = \boldsymbol{Tr}\, u$ *to be smooth periodic functions of the arc length* s. Hence, a natural choice for the basis (37a) is the trigonometric system so that in (38) we have:

$$\psi_0^{(j)} = e^{ij\frac{2\pi s}{S}} \quad \text{and} \quad \psi_1^{(j)} = e^{ij\frac{2\pi s}{S}}. \tag{39}$$

where S is the total length of Γ.

The following consideration is of key importance: even though the system of functions (37a)*) is infinite, the Fourier series* (37b) *for any* $\boldsymbol{\xi}_\Gamma = \boldsymbol{Tr}\, u$ *will converge rapidly because of the smoothness. Hence, to obtain sufficient accuracy one can truncate it after a relatively small number of terms.* Therefore, instead of (37a) we will be considering a finite-dimensional basis

$$\begin{aligned} &\boldsymbol{\psi}_0^{(-M)}, \ldots, \boldsymbol{\psi}_0^{(-3)}, \boldsymbol{\psi}_0^{(-2)}, \boldsymbol{\psi}_0^{(-1)}, \boldsymbol{\psi}_0^{(0)}, \boldsymbol{\psi}_0^{(1)}, \boldsymbol{\psi}_0^{(2)}, \boldsymbol{\psi}_0^{(3)}, \ldots, \boldsymbol{\psi}_0^{(M)}, \\ &\boldsymbol{\psi}_1^{(-M)}, \ldots, \boldsymbol{\psi}_1^{(-3)}, \boldsymbol{\psi}_1^{(-2)}, \boldsymbol{\psi}_1^{(-1)}, \boldsymbol{\psi}_1^{(0)}, \boldsymbol{\psi}_1^{(1)}, \boldsymbol{\psi}_1^{(2)}, \boldsymbol{\psi}_1^{(3)}, \ldots, \boldsymbol{\psi}_1^{(M)} \end{aligned} \tag{40a}$$

composed of functions (38), (39), for which expansion (37b) becomes:

$$\boldsymbol{\xi}_\Gamma = \underbrace{\sum_{-M}^{M} c_{0j} \boldsymbol{\psi}_0^{(j)}}_{(\xi_0,0)} + \underbrace{\sum_{-M}^{M} c_{1j} \boldsymbol{\psi}_1^{(j)}}_{(0,\xi_1)}. \tag{40b}$$

The coefficients c_{0j} and c_{1j} of expansion (40b) will be the actual unknowns for which we will be solving in the method of difference potentials. The choice of M in formulae (40a) and (40b) is discussed in Sect. 4.3 and also in Sect. 5.

4.2 Equation-Based Extension

Next, we extend a given $\boldsymbol{\xi}_\Gamma$ from Γ to γ using the governing equation $\boldsymbol{L}u = f$. In this section we address only the simplest case, whereas in Appendix A we analyze a more general setting.

Consider the Helmholtz equation (9) with a variable k, and assume that the boundary Γ is a circle of radius R centered at the origin (while the discretization grid is Cartesian, see Fig. 2). It will be convenient to recast (9) in polar coordinates:

$$\frac{\partial^2 u}{\partial r^2} + \frac{1}{r}\frac{\partial u}{\partial r} + \frac{1}{r^2}\frac{\partial^2 u}{\partial \theta^2} + k^2(r,\theta)u = f. \tag{41}$$

Let $\boldsymbol{\xi}_\Gamma = (\xi_0, \xi_1)|_\Gamma$ be given on $\Gamma = \{(r,\theta)|r = R,\ 0 \le \theta < 2\pi\}$ so that $\xi_0 = \xi_0(\theta)$ and $\xi_1 = \xi_1(\theta)$. In the vicinity of Γ, we define a new smooth function $v = v(r,\theta)$ by means of the Taylor formula:

$$v(r,\theta) = v(R,\theta) + \sum_{l=1}^{L} \frac{1}{l!}\frac{\partial^l v(R,\theta)}{\partial r^l}(r-R)^l, \tag{42}$$

where the specific choice of L is discussed in Sect. 4.3. The zeroth and first order derivatives in formula (42) are obtained by requiring that $\boldsymbol{Tr}\, v = \boldsymbol{\xi}_\Gamma$:

$$v(R,\theta) = \xi_0(\theta) \quad \text{and} \quad \frac{\partial v(R,\theta)}{\partial r} = \xi_1(\theta). \tag{43}$$

All higher order derivatives in formula (42) are determined with the help of (41) applied to v. The second order radial derivative is obtained immediately from (41) by substituting (43):

$$\frac{\partial^2 u(R,\theta)}{\partial r^2} = -\frac{1}{R}\xi_1(\theta) + \frac{1}{R^2}\frac{\partial^2 \xi_0(\theta)}{\partial \theta^2} - k^2(R,\theta)\xi_0(\theta) + f(R,\theta). \tag{44}$$

The third radial derivative is obtained by differentiating equation (41) once with respect to r and then using (41) again to eliminate $\frac{\partial^2 u}{\partial r^2}$:

$$\begin{aligned}
&\frac{\partial^3 u}{\partial r^3} - \frac{1}{r^2}\frac{\partial u}{\partial r} + \frac{1}{r}\frac{\partial^2 u}{\partial r^2} - \frac{2}{r^3}\frac{\partial^2 u}{\partial \theta^2} + \frac{1}{r^2}\frac{\partial^3 u}{\partial \theta^2 \partial r} + \frac{\partial k^2}{\partial r}u + k^2\frac{\partial u}{\partial r} \\
&\quad = \frac{\partial^3 u}{\partial r^3} - \frac{2}{r^2}\frac{\partial u}{\partial r} - \frac{3}{r^3}\frac{\partial^2 u}{\partial \theta^2} + \frac{1}{r^2}\frac{\partial^3 u}{\partial \theta^2 \partial r} + \left(\frac{\partial k^2}{\partial r} - \frac{k^2}{r}\right)u + k^2\frac{\partial u}{\partial r} + \frac{f}{r} = \frac{\partial f}{\partial r},
\end{aligned} \tag{45}$$

which, after the substitution of expressions (43), yields:

$$\begin{aligned}
\frac{\partial^3 u(R,\theta)}{\partial r^3} &= \frac{2\xi_1(\theta)}{R^2} + \frac{3}{R^3}\frac{\partial^2 \xi_0(\theta)}{\partial \theta^2} - \frac{1}{R^2}\frac{\partial^2 \xi_1(\theta)}{\partial \theta^2} \\
&\quad - \left(\frac{\partial k^2(R,\theta)}{\partial r} - \frac{k^2(R,\theta)}{R}\right)\xi_0(s) - k^2(R,\theta)\xi_1(\theta) - \frac{f(R,\theta)}{R} + \frac{\partial f(R,\theta)}{\partial r}.
\end{aligned} \tag{46}$$

Likewise, the fourth radial derivative is obtained by differentiating (45), eliminating $\frac{\partial^2 u}{\partial r^2}$ with the help of (41), and substituting (43):

$$\begin{aligned}
\frac{\partial^4 u(R,\theta)}{\partial r^4} &= -\frac{6\xi_1(\theta)}{R^3} + \left(\frac{2k^2}{r^2} - \frac{11}{r^4}\right)\frac{\partial^2 \xi_0(\theta)}{\partial \theta^2} + \frac{6}{R^3}\frac{\partial^2 \xi_1(\theta)}{\partial \theta^2} + \frac{1}{R^4}\frac{\partial^4 \xi_0(\theta)}{\partial \theta^4} \\
&\quad - \left(\frac{\partial^2 k^2}{\partial r^2} - \frac{1}{R}\frac{\partial k^2}{\partial r} + \frac{3k^2}{R^2} - k^4 + \frac{1}{R^2}\frac{\partial^2 k^2}{\partial \theta^2}\right)\xi_0(s) - 2\left(\frac{\partial k^2}{\partial r} - \frac{k^2}{R}\right)\xi_1(\theta) \\
&\quad + \left(\frac{3}{R^2} - k^2\right)f - \frac{1}{R}\frac{\partial f}{\partial r} + \frac{\partial^2 f}{\partial r^2} - \frac{1}{R^2}\frac{\partial^2 f}{\partial \theta^2},
\end{aligned} \tag{47}$$

where k^2, f and their derivatives are taken at (R,θ). Additional derivatives are computed similarly.

Once the derivatives for $l = 0,\ldots,L$ in formula (42) have been obtained, one can construct $v(r,\theta)$ in the vicinity of the curve Γ. We emphasize that formula (42) should not be interpreted as an approximation of a known function $v(r,\theta)$ by its truncated Taylor's expansion. Rather, formula (42) is the definition of a new function $v(r,\theta)$. In practice, we need the function $v(r,\theta)$ only at the nodes of the grid boundary γ. We will call it the *equation-based extension* of $\boldsymbol{\xi}_\Gamma$ from Γ to γ:

$$\xi_\gamma = \boldsymbol{Ex}\,\boldsymbol{\xi}_\Gamma \stackrel{\text{def}}{=} v(r,\theta)|_\gamma, \tag{48}$$

where $v(r,\theta)$ is defined by means of formula (42). Later, extension (48) will be applied to the basis functions (40a). This can be done easily because for each basis function (38) since both components are known, see (39), and hence we can begin the Taylor formula (42) as in (43).

In addition to the extension (48), we will need another extension—for the right-hand side f. As indicated in the end of Sect. 3.2, the source term $f(\boldsymbol{x})$ for the boundary value problem (24) may not even be defined anywhere beyond the domain Ω, but the discrete right-hand side $\mathfrak{f}$ needs to be known at the nodes $\mathbb{K}^+ \setminus \mathbb{K}_\Omega$ in order to apply the operator $\boldsymbol{B}^{(h)}$ in formulae (35) and (36). To obtain f at the nodes $\mathbb{K}^+ \setminus \mathbb{K}_\Omega$, which are located close to Γ yet outside Ω, we will also employ the Taylor formula [cf. formula (42)]:

$$f(r,\theta) = f(R,\theta) + \sum_{l=1}^{L-2} \frac{1}{l!} \frac{\partial^l f(R,\theta)}{\partial r^l} (r-R)^l. \tag{49}$$

Since, $f(\boldsymbol{x})$ is defined on Ω, as opposed to $\boldsymbol{\xi}_\Gamma$, which is defined only on Γ, the derivatives of f that enter into formula (49) can be computed as plain one-sided radial derivatives on the interior side of Γ. Then, the extension by means of formula (49) will result in an overall function $f(\boldsymbol{x})$ that will have at least $L-2$ continuous derivatives on a domain somewhat larger than Ω. Note, that since f is on the right-hand side of a second order differential equation, we need two fewer derivatives in the expansion (49) than in (42). The choice of L is discussed in Sect. 4.3.

In Appendix A, we show how to build similar extensions when Γ is an ellipse, and when Γ is a general simple (non-self-intersecting) smooth closed contour on the plane.

4.3 The System of Equations

We have so far introduced a basis for representing $\boldsymbol{\xi}_\Gamma$ on Γ in Sect. 4.1, and we have constructed the extension from Γ to γ in Sect. 4.2 and in Appendix A. *We will now seek $\boldsymbol{\xi}_\Gamma$ in the form* (40b)*, for which the extension* (48)*, or more generally,* (87)*, satisfies the discrete BEP* (35)*.*

We take $\boldsymbol{\xi}_\Gamma$ in the form (40b), where the coefficients c_{0j} and c_{1j}, $j=-M,\ldots,M$, are yet undetermined, extend it from Γ to γ using the equation-based extension (48) or (87), and substitute the resulting ξ_γ into the BEP (35):

$$\begin{aligned}\sum_{-M}^{M} c_{0j} \boldsymbol{P}_\gamma \boldsymbol{E}\boldsymbol{x} \boldsymbol{\psi}_0^{(j)} + \sum_{-M}^{M} c_{1j} \boldsymbol{P}_\gamma \boldsymbol{E}\boldsymbol{x} \boldsymbol{\psi}_1^{(j)} + \boldsymbol{T}\boldsymbol{r}^{(h)} \boldsymbol{G}^{(h)} \boldsymbol{B}^{(h)} \mathfrak{f} \\ = \sum_{-M}^{M} c_{0j} \boldsymbol{E}\boldsymbol{x} \boldsymbol{\psi}_0^{(j)} + \sum_{-M}^{M} c_{1j} \boldsymbol{E}\boldsymbol{x} \boldsymbol{\psi}_1^{(j)},\end{aligned} \tag{50}$$

where we assume that $\mathfrak{f}$ has been obtained with the help of the extension (49) or more generally, (88). We introduce the vector of undetermined coefficients:

$$\boldsymbol{c} = [\underbrace{c_{0-M},\ldots,c_{0M}}_{\boldsymbol{c}_0}, \underbrace{c_{1-M},\ldots,c_{1M}}_{\boldsymbol{c}_1}]^T \tag{51}$$

and the corresponding operator (matrix) of columns $\boldsymbol{P}_\gamma \boldsymbol{Ex}\boldsymbol{\psi}_0^{(j)} - \boldsymbol{Ex}\boldsymbol{\psi}_0^{(j)} \equiv (\boldsymbol{P}_\gamma - \boldsymbol{I}_\gamma)\boldsymbol{Ex}\boldsymbol{\psi}_0^{(j)}$ and $\boldsymbol{P}_\gamma \boldsymbol{Ex}\boldsymbol{\psi}_1^{(j)} - \boldsymbol{Ex}\boldsymbol{\psi}_1^{(j)} \equiv (\boldsymbol{P}_\gamma - \boldsymbol{I}_\gamma)\boldsymbol{Ex}\boldsymbol{\psi}_1^{(j)}$, $j = -M, \ldots, M$:

$$\boldsymbol{Q} = \big[\underbrace{(\boldsymbol{P}_\gamma - \boldsymbol{I}_\gamma)\boldsymbol{Ex}\boldsymbol{\psi}_0^{(-M)}, \ldots, (\boldsymbol{P}_\gamma - \boldsymbol{I}_\gamma)\boldsymbol{Ex}\boldsymbol{\psi}_0^{(M)}}_{\boldsymbol{Q}_0},$$
$$\underbrace{(\boldsymbol{P}_\gamma - \boldsymbol{I}_\gamma)\boldsymbol{Ex}\boldsymbol{\psi}_1^{(-M)}, \ldots, (\boldsymbol{P}_\gamma - \boldsymbol{I}_\gamma)\boldsymbol{Ex}\boldsymbol{\psi}_1^{(M)}}_{\boldsymbol{Q}_1}\big]. \tag{52}$$

The dimension of the vector $\boldsymbol{c}$ is $2(2M+1)$, and the dimension of the matrix $\boldsymbol{Q}$ is $|\gamma| \times 2(2M+1)$, where $|\gamma|$ is the number of nodes in the grid boundary γ. Individual columns of $\boldsymbol{Q}$ are obtained by extending the individual basis functions of (40a) with the help of (87) and then applying the discrete boundary projection $\boldsymbol{P}_\gamma$ of (34). The latter operation involves the solution of the difference AP (30). With the definitions of $\boldsymbol{c}$ and $\boldsymbol{Q}$ given by (51) and (52), (50) can be written as

$$\boldsymbol{Q}\boldsymbol{c} = -\boldsymbol{Tr}^{(h)}\boldsymbol{G}^{(h)}\boldsymbol{B}^{(h)}\mathfrak{f}. \tag{53}$$

Equation (53) should be interpreted as a system of linear algebraic equations for the coefficients $\boldsymbol{c}$ of (51). Once $\boldsymbol{c}$ is known, the extension (87) of the resulting $\boldsymbol{\xi}_\Gamma$ of (40b) will satisfy the discrete BEP (35). Since, the BEP is equivalent only to the governing equation on the domain and does not account for the boundary conditions, then, in addition to system (53), one still needs to consider the boundary condition of (24) in order to uniquely determine $\boldsymbol{c}$.

A key advantage of the proposed methodology is that it offers a very natural and efficient way of handling the boundary conditions. In fact, no approximation of the boundary conditions on the grid is ever required, because the unknown coefficients $\boldsymbol{c}$ directly represent the trace of the continuous solution u at the continuous boundary Γ, see (40b). This trace is a smooth function on the boundary. Hence, integrals, e.g., the far field pattern, can be calculated very accurately.

We first assume that the boundary condition $\boldsymbol{l}_\Gamma u = \phi$ of (24) is of the Dirichlet type:

$$u|_\Gamma = \phi.$$

This is equivalent to specifying the first component of $\boldsymbol{\xi}_\Gamma$, $\xi_0 = \phi$, because the first component of the trace $\boldsymbol{Tr}\,u$ is the Dirichlet data, see formula (13). Therefore, using the partition of $\boldsymbol{c}$ into $\boldsymbol{c}_0$ and $\boldsymbol{c}_1$, see formula (51), we claim that the coefficients $\boldsymbol{c}_0 = [c_{0-M}, \ldots, c_{0M}]^T$ are known and hence system (53) transforms into

$$\boldsymbol{Q}_1\boldsymbol{c}_1 = -\boldsymbol{Q}_0\boldsymbol{c}_0 - \boldsymbol{Tr}^{(h)}\boldsymbol{G}^{(h)}\boldsymbol{B}^{(h)}\mathfrak{f}, \tag{54}$$

where the vector of unknowns is $\boldsymbol{c}_1$, and the matrix $\boldsymbol{Q}$ has been partitioned into $\boldsymbol{Q}_0$ and $\boldsymbol{Q}_1$ according to the partition of $\boldsymbol{c}$, see formula (52).

Likewise, if the boundary condition $\boldsymbol{l}_\Gamma u = \phi$ of (24) is of Neumann type:

$$\left.\frac{\partial u}{\partial n}\right|_\Gamma = \phi,$$

then the second component of $\boldsymbol{\xi}_\Gamma$ can be considered known, $\xi_1 = \phi$, which means that the coefficients $\boldsymbol{c}_1 = [c_{1-M}, \ldots, c_{1M}]^T$ are available, and system (53) becomes

$$\boldsymbol{Q}_0\boldsymbol{c}_0 = -\boldsymbol{Q}_1\boldsymbol{c}_1 - \boldsymbol{Tr}^{(h)}\boldsymbol{G}^{(h)}\boldsymbol{B}^{(h)}\mathfrak{f}, \tag{55}$$

where the vector of unknowns is $\boldsymbol{c}_0$.

Let $\boldsymbol{l}_\Gamma u = \phi$ of (24) be a Robin boundary condition:

$$\alpha u + \beta \frac{\partial u}{\partial n}|_\Gamma = \phi \quad \Leftrightarrow \quad \begin{bmatrix} \alpha & 0 \\ 0 & \beta \end{bmatrix} \boldsymbol{\xi}_\Gamma = \phi,$$

where α and β are two given constants. Then, using orthogonality of the basis functions (40a), one can easily obtain

$$\alpha c_{0j} + \beta c_{1j} = c_{\phi j}, \quad j = -M, \ldots, M, \tag{56}$$

where $c_{\phi j}$ are the coefficients of expanding ϕ with respect to the same basis functions (39). Hence, introducing $\boldsymbol{c}_\phi = [c_{\phi -M}, \ldots, c_{\phi M}]^T$, we can recast system (53) as follows:

$$\left(\boldsymbol{Q}_1 - \frac{\beta}{\alpha} \boldsymbol{Q}_0 \right) \boldsymbol{c}_1 = -\boldsymbol{Q}_0 \boldsymbol{c}_\phi - \boldsymbol{Tr}^{(h)} \boldsymbol{G}^{(h)} \boldsymbol{B}^{(h)} \mathfrak{f}, \tag{57a}$$

where the vector of unknowns is $\boldsymbol{c}_1$, and once it is determined, the remaining coefficients $\boldsymbol{c}_0$ are obtained via (56). Of course, instead of (57a) we could have written

$$\left(\boldsymbol{Q}_0 - \frac{\alpha}{\beta} \boldsymbol{Q}_1 \right) \boldsymbol{c}_0 = -\boldsymbol{Q}_1 \boldsymbol{c}_\phi - \boldsymbol{Tr}^{(h)} \boldsymbol{G}^{(h)} \boldsymbol{B}^{(h)} \mathfrak{f}. \tag{57b}$$

The three systems (54), (55), and (57a), (57b) provide simple examples of how most typical boundary conditions can be handled by the method of difference potentials. It is to be noted that in the framework of the classical boundary integral equations only Dirichlet and Neumann boundary conditions can be handled fairly easily, whereas for Robin boundary conditions the approach is already not as straightforward. The method of difference potentials, on the other hand, enables a straightforward treatment of very general boundary conditions. In particular, in Sect. 6 we outline some non-standard boundary value problems that we plan to address in the future.

Assume now that the coefficients $\boldsymbol{c}$ have been determined by solving system (54), or system (55), or one of the systems (57a), (57b). Then, we can reconstruct $\boldsymbol{\xi}_\Gamma$ using formula (40b), obtain ξ_γ with the help of (87), and finally apply the discrete Green's formula (36), which yields the difference solution $\mathfrak{u}$ on $\mathbb{N}^+$. This completes the solution algorithm. Of course, an important question that still remains is how to actually solve the corresponding system (54), (55), or (57a), (57b).

Each of the systems (54), (55), or (57a), (57b) is a system of $|\gamma|$ linear algebraic equations with $2M+1$ unknowns. As the discretization grid is refined, the quantity $|\gamma|$ increases, see Fig. 3, while M remains fixed. Given that the typical wavelength is on the order of, and often smaller than the characteristic size, and also that at least several grid points per wavelength are required to provide for a sufficient resolution, one can expect that for all "meaningful" grids $|\gamma| > 2M+1$. Therefore, it is natural to solve the corresponding system (54), (55), or (57a), (57b) in the sense of the least squares. We need to emphasize that even though a system with fewer unknowns than equations is formally overdetermined, its solution will be "almost classical"—within the accuracy of approximation, because the original boundary value problem (24) has a unique solution. In this perspective a solution, in the sense of the least squares, can be interpreted as a procedure that offers improved robustness. The least squares solution can be computed using a QR decomposition.

Having completed the description of the algorithm, we still need to discuss how to choose L in the Taylor formula (82) that yields the extension (87), and how to choose M in formulae (40a) and (40b). The choice of L, in particular, is closely related to the rate of grid

convergence of the discrete solution to the continuous solution, as discussed in the following section.

4.4 Accuracy

Approximation of continuous potentials of elliptic operators by the corresponding difference potentials has been investigated by Reznik [38], see also [42]. Below, we outline some of the Reznik's results as they apply to the specific formulation we are studying. The Helmholtz operator on the left-hand side of (9) is an elliptic differential operator $\boldsymbol{L}$ of order $q = 2$. Assume $\boldsymbol{L}$ is approximated by the difference operator $\boldsymbol{L}^{(h)}$ with accuracy $\mathcal{O}(h^p)$. So for a regular scheme we can write

$$\left\| \boldsymbol{L}^{(h)}\mathfrak{u} - (\boldsymbol{L}u)|_{\mathbb{M}_0} \right\|_\delta \le \text{const} \cdot h^p \cdot \|u\|_{2+p+\delta}, \tag{58a}$$

whereas for a compact scheme (Sect. 2) we have

$$\left\| \boldsymbol{L}^{(h)}\mathfrak{u} - \boldsymbol{B}^{(h)}(\boldsymbol{L}u)|_{\mathbb{K}_0} \right\|_\delta \le \text{const} \cdot h^p \cdot \|u\|_{2+p+\delta}. \tag{58b}$$

The norm on the right-hand side of each inequality (58a), (58b) is the continuous Hölder norm of order $2 + p + \delta \equiv q + p + \delta$, and the norm on the left-hand side of each inequality (58a), (58b) is the discrete Hölder norm of order δ on the space $\mathfrak{F}_0$, where $\delta \ge 0$. To define the approximation of the continuous potential by the difference potential, we first need to modify the definitions of the potentials (20) and (32), respectively.

For a given $\boldsymbol{\xi}_\Gamma$, consider the same smooth auxiliary function $w(\boldsymbol{x})$, $\boldsymbol{x} \in \Omega_0$, $\boldsymbol{Tr}\, w = \boldsymbol{\xi}_\Gamma$, as in Sect. 3.1, and the same $g(\boldsymbol{x})$ given by formula (19). In addition, introduce the function $\tilde{w}(\boldsymbol{x})$, $\boldsymbol{x} \in \Omega_0$:

$$\tilde{w}(\boldsymbol{x}) = \begin{cases} w(\boldsymbol{x}), & \boldsymbol{x} \in \Omega, \\ 0, & \boldsymbol{x} \in \Omega_0 \backslash \Omega, \end{cases}$$

that coincides with $w(\boldsymbol{x})$ on Ω and is equal to zero elsewhere on Ω_0. The modified continuous potential

$$\boldsymbol{P}_{\Omega_0}\boldsymbol{\xi}_\Gamma = \tilde{w} - \boldsymbol{G}g \equiv \tilde{w} - \boldsymbol{G}(\boldsymbol{L}w|_\Omega), \quad \boldsymbol{x} \in \Omega_0, \tag{59}$$

is defined on Ω_0 and coincides with the potential $\boldsymbol{P}_\Omega\boldsymbol{\xi}_\Gamma$ of (20) on $\Omega \subset \Omega_0$.

Similarly, for a given ξ_γ consider the same auxiliary grid function $w \in \mathfrak{U}_0$, $\boldsymbol{Tr}^{(h)}\, w = \xi_\gamma$, as in Sect. 3.2, and introduce a modified grid function $\tilde{w} \in \mathfrak{U}_0$:

$$\tilde{w}_n = \begin{cases} w_n, & n \in \mathbb{N}^+, \\ 0, & n \in \mathbb{N}_0 \backslash \mathbb{N}^+, \end{cases}$$

that coincides with w on $\mathbb{N}^+$ and is equal to zero elsewhere on the grid $\mathbb{N}_0$. The modified difference potential

$$\boldsymbol{P}_{\mathbb{N}_0}\xi_\gamma = \tilde{w} - \boldsymbol{G}^{(h)}\big(\boldsymbol{L}^{(h)}w|_{\mathbb{M}^+}\big), \quad n \in \mathbb{N}_0, \tag{60}$$

is defined on $\mathbb{N}_0$ and coincides with the potential $\boldsymbol{P}_{\mathbb{N}^+}\xi_\gamma$ on $\mathbb{N}^+ \subset \mathbb{N}_0$.

Let the extension operator $\boldsymbol{Ex}$ of (87) be defined by the Taylor formula (82) of order $L = q + p \equiv 2 + p$ [see (48) and (42), respectively, for the polar case]. Assume, in addition, that the discrete inverse operator $\boldsymbol{G}^{(h)}$ approximates the continuous inverse operator $\boldsymbol{G}$ with accuracy $\mathcal{O}(h^p)$ weakly, as described in [38], see also [42, Part III, Sect. 1.4]. Then, for a

given continuous density $\boldsymbol{\xi}_\Gamma$, the difference potential $\boldsymbol{P}_{\mathbb{N}_0}\xi_\gamma$ of (60) with the grid density $\xi_\gamma = \boldsymbol{Ex}\boldsymbol{\xi}_\Gamma$ approximates the continuous potential $\boldsymbol{P}_{\Omega_0}\boldsymbol{\xi}_\Gamma$ of (59) in the following sense:

$$\|\boldsymbol{P}_{\Omega_0}\boldsymbol{\xi}_\Gamma - \boldsymbol{P}_{\mathbb{N}_0}\xi_\gamma\|_{2+\varepsilon} \le \text{const} \cdot h^{p-\varepsilon}. \tag{61}$$

In formula (61), ε is arbitrary, with $0 < \varepsilon < 1$, and the norm on the left-hand side of inequality (61) is the discrete Hölder norm of order $2 + \varepsilon = q + \varepsilon$ on the space of grid functions $\mathfrak{U}_0$ defined on $\mathbb{N}_0$. Inequality (61) essentially implies that the values of the potential $\boldsymbol{P}_\Omega\boldsymbol{\xi}_\Gamma$, along with those of its derivatives up to order $q = 2$, are approximated by $\boldsymbol{P}_{\mathbb{N}^+}\xi_\gamma$ everywhere on Ω and up to Γ with accuracy $\mathcal{O}(h^{p-\varepsilon})$, where p is the accuracy of approximation of the continuous operator $\boldsymbol{L}$ by the difference operator $\boldsymbol{L}^{(h)}$ and $\varepsilon > 0$ is arbitrary.

Provided that the density $\boldsymbol{\xi}_\Gamma$ is obtained as described in Sect. 4.3, inequality (61) also implies that the discrete solution $\mathfrak{u}$ *given by (36) will converge as $h \to 0$ to the continuous solution u of the corresponding problem (24) with the same rate and in the sense of the same norm as in (61).*

In our experiments, we have additionally determined that the estimate $L = 2 + p \equiv q + p$ is not sharp, and a lower value of L can, in practice, be chosen. We have used three different schemes: the standard (i.e., non-compact) second order accurate central difference scheme, a fourth order accurate compact scheme (10) applied to both constant and variable coefficients, and a sixth order accurate compact scheme of [48] for constant coefficients, see Sect. 5. In each case, we have found that taking $L = p$ already guarantees the design rate of grid convergence. *Therefore, in all our simulations we took $L = 2$ for the second order scheme, $L = 4$ for the fourth order scheme, and $L = 6$ for the sixth order scheme.*

The value of M in formulae (40a), (40b) that provides sufficient accuracy is, of course, formulation dependent. For smooth solutions, however, the error due to the truncation of the Fourier series [i.e., due to the replacement of (37b) by (40b)] may typically be driven to machine zero already for M on the order of a few tens. This accuracy normally exceeds any accuracy that one would expect to obtain on the grid, and so in practice the value of M can be taken even smaller.

Therefore, there are two strategies for choosing the value of M. The first one is to fix it at a given level, e.g., the level that would guarantee the machine precision of the expansion at the boundary. In this case, M is not related to the size of the discretization grid. It is chosen once for a given problem, and then the convergence of the method is monitored by refining the grid while keeping the value of M fixed. This is the strategy adopted in the current paper, see Sect. 5. In the other strategy the value of M is chosen so as to have the accuracy of the expansion at the boundary match that of the approximation on the grid inside the domain. In this case, M will depend on the grid size, but will always be smaller than the fixed value that guarantees machine precision. Therefore, this approach offers additional efficiency. Its practical implementation will be discussed in a future publication.

4.5 Summary of Computational Procedure

The key steps of the proposed computational algorithm are the following:

1. Choose the discrete AP (30). Its domain Ω_0 should contain Ω, the grid $\mathbb{N}_0$ should provide sufficient resolution [through its sub-grid $\mathbb{N}^+$, see formula (31)], and the boundary condition $\mathfrak{u} \in \mathfrak{U}_0$ should guarantee unique solvability and well-posedness. Other than that, there are no constraints. The AP should be formulated so as to enable an easy and efficient numerical solution.

(a) As recommended in Sect. 3.2, Ω_0 should be a regular domain, such as a rectangle or a disk, and $\mathbb{N}^0$ should be a regular structured grid, e.g., uniform Cartesian or polar.
(b) If the coefficients of the governing equation are constant, the AP (30) can be solved by separation of variables/FFT, and its boundary condition $\mathfrak{u} \in \mathfrak{U}_0$ should be chosen accordingly (for a compact scheme we do not need more boundary conditions than for the differential equation).
(c) In the case of variable coefficients, the AP can be solved either by a sparse LU decomposition or by an iterative method.

2. Introduce the finite-dimensional representation (39), (40a), (40b) for $\boldsymbol{\xi}_\Gamma$ on Γ.
   (a) Select M by expanding the given boundary data ϕ, see formula (24), with respect to the chosen system of functions (37a), (38), (39), and truncating the expansion at the machine precision level.
   (b) It is to be expected that larger values of M will be needed for higher frequencies/shorter wavelengths.
3. Build the required grid sets according to the definition (31).
4. For each basis function of (40a), construct its equation-based extension from Γ to γ using (82), (87).
5. Apply the discrete boundary projection $\boldsymbol{P}_\gamma$ of (34) to the resulting extension ξ_γ, which requires a single solution of the discrete AP (30), i.e., the computation of $\boldsymbol{G}^{(h)}(\boldsymbol{L}^{(h)} w|_{\mathbb{M}^+})$, where $\boldsymbol{Tr}^{(h)} w = \xi_\gamma$.
6. From $\boldsymbol{P}_\gamma \xi_\gamma$, compute the corresponding column of the matrix $\boldsymbol{Q}$ of (52).
7. Implement the extension (88) for the source function f, evaluate $\boldsymbol{B}^{(h)}\mathfrak{f}$, and compute $\boldsymbol{G}^{(h)}\boldsymbol{B}^{(h)}\mathfrak{f}$,—this involves one more solution of the discrete AP (30).
8. Depending on the specific formulation of the boundary value problem (24), set up the corresponding linear system (54), (55), or (57a), (57b) (Dirichlet, Neumann, or Robin boundary conditions, respectively).
9. Solve the resulting system (54), (55), or (57a), (57b) using the QR decomposition.
10. Having obtained the solution of the linear system, i.e., the vector of coefficients $\boldsymbol{c}$ of (51):
    (a) Use formula (40b) to compute the actual boundary trace of the solution u to problem (24), $\boldsymbol{\xi}_\Gamma = \boldsymbol{Tr}\, u$.
    (b) Extend $\boldsymbol{\xi}_\Gamma$ from Γ to γ with the help of (82), (87).
    (c) Obtain the solution $\mathfrak{u}$ on the grid $\mathbb{N}^+$ using the generalized discrete Green's formula (36).
    (d) Evaluation of the difference potential (32) that enters into (36) requires one additional solution of the difference AP (30).

4.6 Complexity

The key contribution to the overall complexity of the proposed algorithm is the repeated solution of the discrete AP (30). Altogether, it needs to be solved a maximum of $2(2M + 1) + 2 = 4(M + 1)$ times. Therefore, the value of M impacts strongly on the efficiency of the method. However, only the right-hand side of the AP changes, whereas the operator remains the same. In the case of constant coefficients, each of the $4(M + 1)$ requires a FFT solve which has a log-linear complexity with respect to the dimension (i.e., the number of nodes) $|\mathbb{N}_0|$ of the grid $\mathbb{N}_0$. In the case of variable coefficients, the overall complexity will be that of a single sparse LU decomposition of a matrix of dimension $|\mathbb{N}_0| \times |\mathbb{N}_0|$ plus $4(M + 1)$ backward substitutions, each with linear complexity with respect to $|\mathbb{N}_0|$.

In the case of variable coefficients, one can also use an iterative solver. In 3D, an iterative solver becomes a necessity even in the case of constant coefficients. Since we require the

solution of a number of systems with the same matrix and different right-hand sides, we could use the block version of many of the Krylov iterative schemes; see, for example, [11, 12, 17]. Alternately, we can use the iterative scheme Risolv of [52]. Then, one needs to find the optimal parameters of the algorithm only once independent of the RHS. Let N_{nz} be the number of non-zero entries in the system matrix that has the dimension $|\mathbb{N}_0| \times |\mathbb{N}_0|$, N_{K} be the dimension of the Krylov subspace, and N_{A} be the number of times we apply the Arnoldi algorithm. Then the total amount of work for the first solve, i.e., for one RHS, is approximately $N_{\mathrm{A}} \times N_{\mathrm{K}} \times N_{\mathrm{nz}} + N_{\mathrm{A}} \times \frac{N_{\mathrm{K}}^2}{2}|\mathbb{N}_0|$. For each subsequent solve the total work is approximately $N_{\mathrm{A}} \times N_{\mathrm{K}} \times N_{\mathrm{nz}}$. Hence, it no longer depends on $N_{\mathrm{K}}^2|\mathbb{N}_0|$, which means that the dependence on the dimension $|\mathbb{N}_0|$ of the system matrix disappears, and the dependence on the dimension N_{K} of the Krylov subspace becomes linear rather than quadratic. Regarding preconditioning of the Helmholtz equation, see, e.g. [13–16].

Another contribution to the overall complexity is that of the QR decomposition. If the modified Gram-Schmidt algorithm is used, then the corresponding cost is about $2(2M+1)^2|\gamma|$ operations, where for the current two-dimensional setting $|\gamma| \sim \sqrt{|\mathbb{N}_0|}$. The cost of all other components of the algorithm, see Sect. 4.5, is negligible. In the simulations reported below (Sect. 5), as the discretization grid is refined only the quantities $|\mathbb{N}_0|$ and $|\gamma|$ increase, whereas M stays the same.

5 Numerical Experiments

5.1 Schemes of Various Accuracy for the Constant Coefficient Helmholtz Equation

We first solve the interior Dirichlet problem for the constant coefficient homogeneous Helmholtz equation:

$$\begin{aligned} &\Delta u + k^2 u = 0 \quad \text{on } \Omega, \\ &u|_\Gamma = \phi, \end{aligned} \tag{62}$$

on the domain Ω which is a disk of radius $R = 3$ centered at the origin. The auxiliary problem (see Definition 1) is formulated on a larger square

$$\Omega_0 = \left\{(x, y) \mid -\pi \le x,\ y \le \pi\right\} \supset \Omega,$$

and consists of solving the inhomogeneous Helmholtz equation

$$\Delta v + k^2 v = g$$

subject to the zero Dirichlet boundary condition:

$$v|_{\partial\Omega_0} = 0.$$

To avoid resonances and guarantee uniqueness of the solution to the AP, we require that $k^2 \neq l^2 + m^2$, where l and m are any two integer numbers. The AP is solved by a sparse LU decomposition.

We take the test solution of problem (62) in the form of a plane wave:

$$u(x, y) = e^{i(k_x x + k_y y)}, \quad \text{where } k_x^2 + k_y^2 = k^2, \tag{63}$$

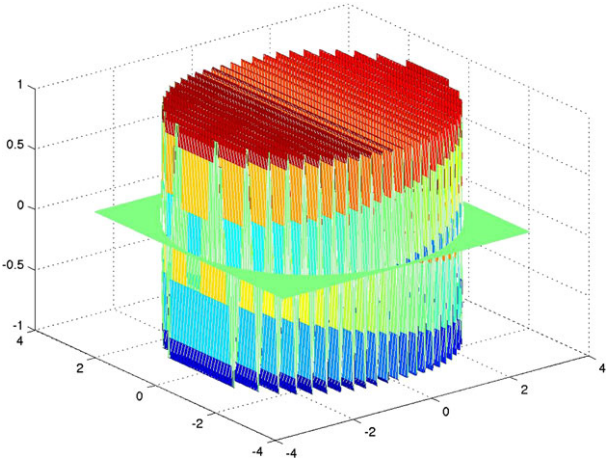

Fig. 4 Real part of the test solution (63) for $k = 25.6$

so that the boundary data in (62) become

$$\phi(\theta) = e^{iR(k_x \cos\theta + k_y \sin\theta)}, \tag{64}$$

where θ is the polar angle. The specific values that we choose are: $k_x = \frac{4}{5}k$ and $k_y = \frac{3}{5}k$.

To discretize the Helmholtz equation, we use a uniform in both directions Cartesian grid with size h on the square Ω_0 (the domain of the AP). In doing so, the circular boundary Γ of the domain Ω, i.e., the domain of the original problem (62), does not conform to the grid. The Helmholtz equation is discretized by means of the following three schemes:

1. The standard central difference second order accurate scheme on the five-node stencil;
2. The fourth order accurate compact scheme of Sect. 2.2, which uses the nine-node stencil shown in Fig. 1 (left) [the equation in (62) is homogeneous, and no stencil is needed for the right-hand side]. For the case of $k = \text{const}$, the scheme simplifies compared to formula (10);
3. The sixth order accurate compact scheme of [48], which uses the same nine-node stencil.

The goals of the computations below are to demonstrate the design order of grid convergence of the numerical solution to the exact solution for a non-conforming boundary, and to see what minimum number of Taylor derivatives is needed in formula (42) to maintain this convergence for every order of accuracy. An additional goal is to show how the pollution effect [1, 4, 23] manifests itself.

The grid convergence is studied by solving on a sequence of grids of increasing dimension: $2^d \times 2^d$, from 16×16 to the maximum of 1024×1024, so that for a given d the grid size $h = \frac{2\pi}{2^d} = \pi 2^{1-d}$, and it is halved every time the grid dimension is increased.

We have solved problem (62) for five different values of the wavenumber k: 1, 3, 6.7, 12.8, and 25.6. For the highest k that we have considered, the test solution (63) already exhibits a fair amount of oscillations on the domain Ω—about 25 full wavelengths along the diameter, as shown in Fig. 4. The results of computations for all k's are presented in Tables 1 through 5.

The dimension M of the basis (40a) is chosen by Fourier transforming the boundary data (64) of problem (62) and truncating the series at the machine precision level (`real*8`). The resulting values of M for every k are provided in the captions to Tables 1, 2, 3, 4, 5. We see that M increases as k increases. This is not surprising, as the solution becomes more

Table 1 Grid convergence for the wavenumber $k = 1$ and the dimension of the basis (40a) $M = 17$. Note that the apparent breakdown of convergence of higher order schemes on finer grids is due to the loss of significant digits, as the absolute levels of the error become very small and approach the machine zero

Grid	Scheme					
	2nd order ctr. difference		4th order compact		6th order compact	
	$\|u - u_{num}\|_\infty$	Conv. rate	$\|u - u_{num}\|_\infty$	Conv. rate	$\|u - u_{num}\|_\infty$	Conv. rate
16×16	3.474855×10^{-2}	–	4.590536×10^{-4}	–	3.626766×10^{-6}	–
32×32	5.346252×10^{-3}	2.7004	5.163260×10^{-6}	6.4742	8.250530×10^{-9}	8.7800
64×64	1.238241×10^{-3}	2.1102	1.704410×10^{-7}	4.9209	6.486869×10^{-11}	6.9908
128×128	3.001289×10^{-4}	2.0446	9.090205×10^{-9}	4.2288	1.112940×10^{-12}	5.8651
256×256	7.389904×10^{-5}	2.0220	3.272063×10^{-10}	4.7960	2.343009×10^{-12}	−1.0740
512×512	1.835138×10^{-5}	2.0097	2.457055×10^{-11}	3.7352	7.287204×10^{-12}	−1.6370
1024×1024	4.571995×10^{-6}	2.0050	3.070920×10^{-11}	−0.3217	2.411052×10^{-11}	−1.7262

Table 2 Grid convergence for the wavenumber $k = 3$ and the dimension of the basis (40a) $M = 28$

Grid	Scheme					
	2nd order ctr. difference		4th order compact		6th order compact	
	$\|u - u_{num}\|_\infty$	Conv. rate	$\|u - u_{num}\|_\infty$	Conv. rate	$\|u - u_{num}\|_\infty$	Conv. rate
16×16	2.157031	–	1.093211	–	6.252035×10^{-2}	–
32×32	2.212195×10^{-1}	3.2855	1.491703×10^{-3}	9.5174	1.905533×10^{-5}	11.6799
64×64	6.296501×10^{-2}	1.8129	4.695925×10^{-5}	4.9894	2.743013×10^{-7}	6.1183
128×128	1.621645×10^{-2}	1.9571	2.736886×10^{-6}	4.1008	3.956555×10^{-9}	6.1154
256×256	4.049416×10^{-3}	2.0017	1.612331×10^{-7}	4.0853	5.830238×10^{-11}	6.0845
512×512	1.008930×10^{-3}	2.0049	9.823236×10^{-9}	4.0368	1.288003×10^{-12}	5.5003
1024×1024	2.515190×10^{-4}	2.0041	6.235303×10^{-10}	3.9777	7.870095×10^{-12}	−2.6112

Table 3 Grid convergence for the wavenumber $k = 6.7$ and the dimension of the basis (40a) $M = 43$

Grid	Scheme					
	2nd order ctr. difference		4th order compact		6th order compact	
	$\|u - u_{num}\|_\infty$	Conv. rate	$\|u - u_{num}\|_\infty$	Conv. rate	$\|u - u_{num}\|_\infty$	Conv. rate
16×16	8.228113	–	7.976387	–	1.459757×10	–
32×32	4.299483	0.9364	1.001469×10^{-1}	6.3155	1.071898×10^{-2}	10.4113
64×64	1.933134	1.1532	4.111705×10^{-3}	4.6062	1.345917×10^{-4}	6.3154
128×128	3.065574×10^{-2}	2.6567	2.420283×10^{-4}	4.0865	1.845635×10^{-6}	6.1883
256×256	7.028536×10^{-3}	2.1249	1.488596×10^{-5}	4.0232	2.757929×10^{-8}	6.0644
512×512	1.861682×10^{-3}	1.9166	9.101549×10^{-7}	4.0317	4.192718×10^{-10}	6.0396
1024×1024	4.726287×10^{-4}	1.9778	5.640010×10^{-8}	4.0123	1.170244×10^{-11}	5.1630

Table 4 Grid convergence for the wavenumber $k = 12.8$ and the dimension of the basis (40a) $M = 66$

Grid	Scheme					
	2nd order ctr. difference		4th order compact		6th order compact	
	$\|u - u_{num}\|_\infty$	Conv. rate	$\|u - u_{num}\|_\infty$	Conv. rate	$\|u - u_{num}\|_\infty$	Conv. rate
16×16	3.135403×10	–	7.284196×10	–	9.174488×10	–
32×32	2.693366×10	0.2192	4.960223	3.8763	1.344958×10	2.7701
64×64	8.177246	0.2192	1.233802	2.0073	8.032610×10^{-2}	7.3875
128×128	1.095035×10	−0.4213	3.200884×10^{-2}	5.2685	1.039313×10^{-3}	6.2722
256×256	2.603452	2.0725	2.048553×10^{-3}	3.9658	1.395774×10^{-5}	6.2184
512×512	6.781712×10^{-1}	1.9407	1.277844×10^{-4}	4.0028	2.125559×10^{-7}	6.0371
1024×1024	1.448771×10^{-1}	2.2268	7.718401×10^{-6}	4.0493	3.172309×10^{-9}	6.0662

Table 5 Grid convergence for the wavenumber $k = 25.6$ and the dimension of the basis (40a) $M = 111$

Grid	Scheme					
	2nd order ctr. difference		4th order compact		6th order compact	
	$\|u - u_{num}\|_\infty$	Conv. rate	$\|u - u_{num}\|_\infty$	Conv. rate	$\|u - u_{num}\|_\infty$	Conv. rate
16×16	1.144291×10^{2}	–	2.065713×10^{3}	–	1.175546×10^{4}	–
32×32	4.851901×10	1.2378	8.885777×10	4.5390	4.453015×10	8.0443
64×64	1.280298×10	1.9221	2.818431	4.9785	1.219721×10	1.8682
128×128	1.901798×10	−0.5709	4.128656×10^{-1}	2.7711	1.039313×10^{-3}	5.5781
256×256	1.448009×10	0.3933	1.737760×10^{-1}	1.2484	1.973019×10^{-3}	7.0158
512×512	4.563927	1.6657	4.317500×10^{-3}	5.3309	2.883989×10^{-5}	6.0962
1024×1024	3.892365	0.2296	2.603055×10^{-4}	4.0519	4.398634×10^{-7}	6.0349

oscillatory;[1] for example, our highest $k = 25.6$ corresponds to over 75 full wavelengths along the circumference $R = 3$. On the other hand, we also see in Tables 1 through 5 that the accuracy actually achieved on the grid is often orders of magnitude less than the machine precision. This indicates that the chosen M may be superfluous, and the same accuracy of the solution can be obtained using a smaller basis (40a) at a lower computational cost. For example, the fourth order computations presented in Table 5 ($k = 25.6$) were repeated for $M = 94$ (instead of $m = 111$) with the same results.

Altogether, Tables 1, 2, 3, 4, 5 show that for every scheme we have tested, the proposed methodology guarantees the design rate of grid convergence for a non-conforming boundary and a Cartesian grid.

Note, that all the computations presented in Tables 1, 2, 3, 4, 5 were conducted for $L = p$, i.e., for the number of Taylor derivatives in formula (42) equal to the order of accuracy of the scheme. This value of L is already lower than $L = 2 + p$ predicted by the theoretical estimate of [38]. To see whether or not our current choice of L can be improved further, we have conducted similar computations, but for an even smaller number of Taylor derivatives, $L = p - 1$. In Table 6, we present the results for $k = 3$. The data show a certain deterioration of the convergence rate (cf. Table 2), which indicates that the number of terms L in the

[1] Convergence of the Fourier series remains exponential due to the smoothness, but the constants become larger.

Table 6 Grid convergence for the wavenumber $k = 3$ and the dimension of the basis (40a) $M = 28$

Grid	Scheme					
	2nd order ctr. difference		4th order compact		6th order compact	
	$\|u - u_{num}\|_\infty$	Conv. rate	$\|u - u_{num}\|_\infty$	Conv. rate	$\|u - u_{num}\|_\infty$	Conv. rate
16×16	3.752407	–	2.907471×10^{-1}	–	7.342967×10^{-2}	–
32×32	2.290364×10^{-1}	4.0342	1.010567×10^{-2}	4.8465	1.432143×10^{-4}	9.0020
64×64	6.503502×10^{-2}	1.8163	8.516129×10^{-4}	3.5688	3.976092×10^{-6}	5.1707
128×128	1.990979×10^{-2}	1.7077	7.105160×10^{-5}	3.5833	9.373316×10^{-8}	5.4066
256×256	5.743664×10^{-3}	1.7934	4.898880×10^{-6}	3.8583	1.693751×10^{-9}	5.7903
512×512	2.130201×10^{-3}	1.4310	3.736573×10^{-7}	3.7127	3.099734×10^{-11}	5.7719
1024×1024	4.835611×10^{-4}	2.1392	2.310974×10^{-8}	4.0151	7.720891×10^{-12}	2.0053

equation-based extension formulae (42), (48) should not be taken any lower than the order of accuracy p of the scheme.

5.2 Variable Wavenumber Helmholtz Equation with Fourth Order Accuracy

We now use the fourth order accurate compact scheme (10) to solve the inhomogeneous Helmholtz equation (9) with variable wavenumber inside circles and ellipses, subject to the Dirichlet or Neumann boundary conditions. The goal of the computations is to demonstrate the capability of the proposed method to address variable coefficients and various types of the boundary conditions, and again, to show the design order of grid convergence for non-conforming boundaries (the discretization grid is always Cartesian). The domain $\Omega \subset \Omega_0$ is either a disk of radius $R = 1$ centered at the origin, or the interior of the ellipse with the major semi-axis $a = 1$ and minor semi-axis $b = 1/2$, see formula (69).

The Helmholtz equation (9) that we solve on the domain Ω has a variable wavenumber k. For the case of the disk we choose

$$k = k_0 e^{-10(r-r_0)^6 r^6 \cos\theta}, \tag{65}$$

and for the case of the ellipse we take

$$k = k_0 e^{-10(r-r_0)^6 r^6}, \tag{66}$$

where r is the polar radius and θ is the polar angle and the parameter $r_0 = 1.6$. The profiles of k are schematically shown in Fig. 5.

In either case, circle or ellipse, the exact solution is chosen in the form:

$$u = e^{ikx}. \tag{67}$$

Since k is variable, see formulae (65) and (66), this solution is not a plane wave, as shown in Fig. 6. The corresponding right-hand side $f(x, y)$ in formula (9) is obtained by backward engineering, i.e., by substituting u given by (67) into the left-hand side of the Helmholtz equation.

The boundary condition at $\Gamma = \partial\Omega$ for the Helmholtz equation (9) can be of either Dirichlet or Neumann type. The required boundary data are also obtained by backward engineering, i.e., by taking the trace of either the solution u itself or its normal derivative $\frac{\partial u}{\partial n}$ at the boundary Γ.

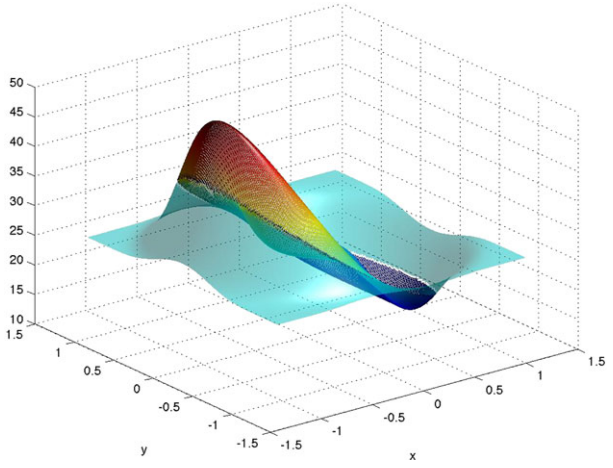

(a) Ω is a circle, formula (65)

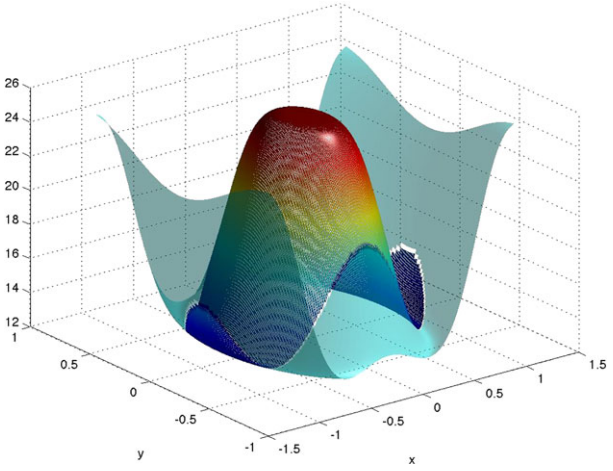

(b) Ω is an ellipse, formula (66)

Fig. 5 Profiles of the variable wavenumber k on Ω_0 for $k_0 = 25$; the part inside Ω is emphasized

In the case of Ω being a disk of radius $R = 1$, the AP (see Definition 1) is formulated on the square

$$\Omega_0 = \{(x, y) \mid -1.2 \le x, y \le 1.2\}$$

with the following boundary conditions:

$$v = 0 \quad \text{at } y = \pm 1.2,$$

and

$$\frac{dv}{dx} + iv = 0 \quad \text{at } x = 1.2 \quad \text{and} \quad \frac{dv}{dx} - iv = 0 \quad \text{at } x = -1.2. \tag{68}$$

The pair of complex boundary conditions (68) guarantees that regardless of k there will be no resonances in the solution of the AP on the square Ω_0.

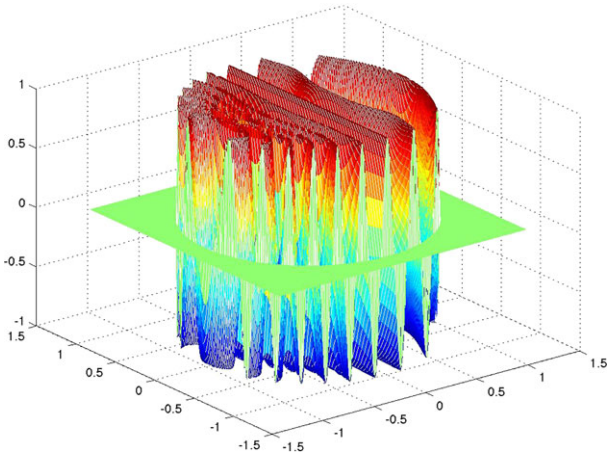

(a) Circle

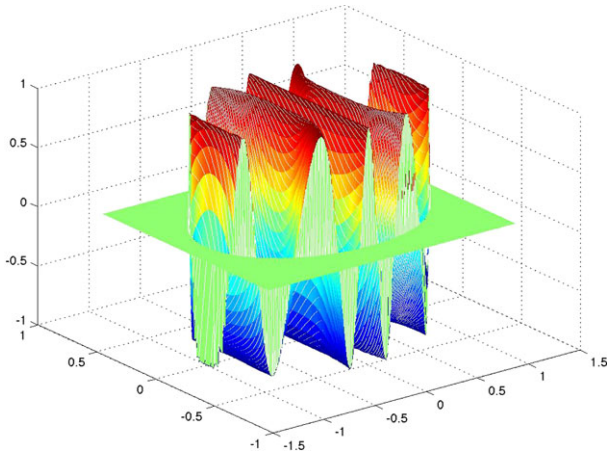

(b) Ellipse

Fig. 6 Real part of the test solution (67) for $k_0 = 25$

In the case of the ellipse, the AP is formulated on the rectangle

$$\Omega_0 = \{(x, y) \mid -1.2 \le x \le 1.2,\ -0.7 \le y \le 0.7\}$$

with the boundary conditions:

$$v = 0 \quad \text{at } y = \pm 0.7,$$

and the same complex boundary conditions (68) at $x = \pm 1.2$.

Similar to Sect. 5.1, the AP is discretized on a sequence of uniform in each direction Cartesian grids of dimension $2^d \times 2^d$, with the maximum of 2048×2048. For a given d, the grid size in the case of a square is $h = \frac{2.4}{2^d}$, and the grid sizes in the case of a rectangle are $h_x = \frac{2.4}{2^d}$ and $h_y = \frac{1.4}{2^d}$. The grid sizes are halved every time d is incremented by 1, which is convenient for studying the convergence. As in Sect. 5.1, the AP is also solved by the sparse LU decomposition.

Table 7 Grid convergence of the solution to the Dirichlet problem for the ellipse $a = 1$, $b = \frac{1}{2}$. Variable coefficient Helmholtz equation (9) and a fourth order compact scheme (10)

Grid	Ellipse					
	$k_0 = 5$, $M = 42$		$k_0 = 15$, $M = 54$		$k_0 = 25$, $M = 67$	
	$\|u - u_{num}\|_\infty$	Conv. rate	$\|u - u_{num}\|_\infty$	Conv. rate	$\|u - u_{num}\|_\infty$	Conv. rate
16×16	8.283939	–	3.950658×10	–	5.206655×10	–
32×32	1.978583×10^{-2}	8.7097	6.015599×10^{-1}	6.0372	3.388063×10	0.6199
64×64	3.104902×10^{-4}	5.9938	7.001777×10^{-3}	6.4248	8.662025×10^{-2}	8.6115
128×128	1.659692×10^{-5}	4.2256	7.492233×10^{-4}	3.2243	5.811711×10^{-3}	3.8977
256×256	5.597237×10^{-7}	4.8901	2.551093×10^{-5}	4.8762	3.104959×10^{-4}	4.2263
512×512	2.094249×10^{-8}	4.7402	1.551669×10^{-6}	4.0392	1.881038×10^{-5}	4.0450
1024×1024	6.565249×10^{-10}	4.9954	9.538440×10^{-8}	4.0239	1.160326×10^{-6}	4.0189
2048×2048	2.761463×10^{-11}	4.5713	5.897927×10^{-9}	4.0155	7.200706×10^{-8}	4.0102

Table 8 Grid convergence of the solution to the Dirichlet problem for the circle $R = 1$. Variable coefficient Helmholtz equation (9) and a fourth order compact scheme (10)

Grid	Circle					
	$k_0 = 5$, $M = 32$		$k_0 = 15$, $M = 54$		$k_0 = 25$, $M = 73$	
	$\|u - u_{num}\|_\infty$	Conv. rate	$\|u - u_{num}\|_\infty$	Conv. rate	$\|u - u_{num}\|_\infty$	Conv. rate
16×16	3.038830	–	1.517016×10^2	–	1.571341×10^2	–
32×32	2.231693×10^{-2}	7.0892	3.324707	5.5119	1.304138×10	3.5908
64×64	1.405180×10^{-3}	3.9893	1.032080×10^{-1}	5.0096	2.744285	2.2486
128×128	7.302520×10^{-5}	4.2662	5.746378×10^{-3}	4.1668	5.751020×10^{-2}	5.5765
256×256	4.465171×10^{-6}	4.0316	3.454849×10^{-4}	4.0560	3.678247×10^{-3}	3.9667
512×512	2.701632×10^{-7}	4.0468	2.125100×10^{-5}	4.0230	2.265488×10^{-4}	4.0211
1024×1024	1.680068×10^{-8}	4.0072	1.321587×10^{-6}	4.0072	1.405292×10^{-5}	4.0109
2048×2048	1.040726×10^{-9}	4.0129	8.239623×10^{-8}	4.0035	8.745530×10^{-7}	4.0062

Numerical results of solving the Dirichlet problem for the variable coefficient Helmholtz equation (9) are presented in Table 7 in the case of an ellipse and in Table 8 in the case of a circle. For the range of k's that we have investigated, $k_0 = 5$, 15, and 25, the data in the tables fully corroborate the design fourth order rate of grid convergence for the compact Cartesian scheme (10) when the non-conforming boundaries are handled by the method of difference potentials.

Similar numerical results for the Neumann problem are presented in Table 9 for the ellipse and in Table 10 for the circle. As in the case of the Dirichlet problem, the data in the tables fully corroborate the design fourth order rate of grid convergence of the proposed methodology.

6 Conclusions

We have described a combined implementation of the method of difference potentials along with the compact high order accurate finite difference schemes for the numerical solution of

Table 9 Grid convergence of the solution to the Neumann problem for the ellipse $a = 1$, $b = \frac{1}{2}$. Variable coefficient Helmholtz equation (9) and a fourth order compact scheme (10)

Grid	Ellipse					
	$k_0 = 5$, $M = 42$		$k_0 = 15$, $M = 54$		$k_0 = 25$, $M = 67$	
	$\|u - u_{num}\|_\infty$	Conv. rate	$\|u - u_{num}\|_\infty$	Conv. rate	$\|u - u_{num}\|_\infty$	Conv. rate
16×16	4.267776×10	–	1.772119×10^2	–	3.649132×10^2	–
32×32	9.712126×10^{-2}	8.7795	2.316084	6.2576	$3.309569 - \times 10$	3.4628
64×64	7.548180×10^{-3}	3.6856	6.203786×10^{-2}	5.2224	1.573478×10^{-2}	7.7165
128×128	4.486249×10^{-4}	4.0725	4.713176×10^{-3}	3.7184	1.589413×10^{-3}	3.3074
256×256	2.486193×10^{-5}	4.1735	2.419222×10^{-4}	4.2841	6.383346×10^{-4}	4.6380
512×512	1.372890×10^{-6}	4.1787	1.635393×10^{-5}	3.8868	4.329843×10^{-5}	3.8819
1024×1024	9.028545×10^{-8}	3.9266	9.750050×10^{-7}	4.0681	2.425497×10^{-6}	4.1580
2048×2048	5.198146×10^{-9}	4.1184	6.308512×10^{-8}	3.9500	1.584606×10^{-8}	3.9361

Table 10 Grid convergence of the solution to the Neumann problem for the circle $R = 1$. Variable coefficient Helmholtz equation (9) and a fourth order compact scheme (10)

Grid	Circle					
	$k_0 = 5$, $M = 32$		$k_0 = 15$, $M = 54$		$k_0 = 25$, $M = 73$	
	$\|u - u_{num}\|_\infty$	Conv. rate	$\|u - u_{num}\|_\infty$	Conv. rate	$\|u - u_{num}\|_\infty$	Conv. rate
16×16	1.188942	–	8.839874×10	–	1.713283×10^2	–
32×32	1.801846×10^{-2}	6.0441	6.391570×10	5.5119	7.346974×10	1.2215
64×64	1.245872×10^{-3}	3.8542	3.179250×10^{-1}	5.0096	2.938586	4.6440
128×128	5.731111×10^{-5}	4.4422	3.336937×10^{-2}	4.1668	4.978325×10^{-2}	5.8833
256×256	4.343596×10^{-6}	3.7219	2.037841×10^{-3}	4.0560	2.970674×10^{-3}	4.0668
512×512	2.118921×10^{-7}	4.3575	1.218354×10^{-4}	4.0230	1.810039×10^{-4}	4.0367
1024×1024	1.467516×10^{-8}	3.8519	7.567901×10^{-6}	4.0072	1.144116×10^{-5}	3.9837
2048×2048	8.996365×10^{-10}	4.0279	4.64726×10^{-7}	4.0035	7.144455×10^{-7}	4.0013

wave propagation problems in the frequency domain. The governing Helmholtz equation is approximated on a regular structured grid, which is efficient and entails a low computational complexity. At the same time, the method guarantees no loss of accuracy for curvilinear non-conforming boundaries, and can also handle variable coefficients that describe a non-homogeneous medium. As such, the resulting method provides a viable alternative to both BEM and high order FEM.

The performance of the method and, in particular, its design high order accuracy, has been corroborated numerically by solving a variety of 2D interior Helmholtz problems, including those with variable coefficients, on the Cartesian grid but for the boundaries shaped as circles and ellipses.

Among other advantages of the proposed methodology are its capability to accurately reconstruct the solution and/or its normal derivative directly at the boundary (without having to interpolate and/or use one-sided differences, such as in conventional FD, and with no additional developments needed in FEM, see, e.g., [9]), the absence of any singular integrals or similar constructs, the minimum number of unknowns that characterize the discrete

solution—just one per grid node, and the same number of boundary conditions needed for the scheme as that needed for the underlying differential equation.

In the near future, we plan to apply the proposed methodology to exterior problems. This will involve constructing the auxiliary problems (see Definitions 1 and 2) with the appropriate artificial boundary conditions (ABCs), see [55]. For the constant coefficient 2D Helmholtz equation (typical for the far field), the AP can be conveniently formulated using polar coordinates, which enables a natural and efficient implementation of the exact non-local ABCs in the Fourier space. In addition, we plan to extend the proposed methodology from solving the interior and exterior scattering problems separately to solving the combined reflection/transmission problems. The latter formulation will involve a joint solution of the interior and exterior Calderon's BEPs constructed at the interface between the interior and exterior sub-regions.

Together with extending the algorithm to a broader range of formulations, we will explore alternative strategies for choosing M—the dimension of the basis used for representing the solution at the boundary Γ (40b). Specifically, we will include the capability of reducing M in accordance with the expected accuracy on the grid. In addition to that, we will examine the possibility of using other bases, beyond the trigonometric system (37a), (38), (39). We expect that applying the ideas of reduced order modeling [19] (or, similarly, principal component analysis or proper orthogonal decomposition) will help us further reduce the dimension of the basis on Γ. Other bases may be convenient to use in the case of piece-wise parametrization (see below).

We will also consider domains of a more general shape (beyond circles and ellipses), first those with a smooth boundary, and subsequently those with the corners. Arbitrary smooth boundaries will require a more general construction of the extension operators (see Appendix A), whereas corners will require special attention to possible singularities of the solution. In either case, it may be more convenient to use a piece-wise parametrization of the boundary rather that a global parametrization. In the case of corners, piece-wise parametrization is a must, but it may still be very useful to have even if the boundary is smooth, for example, when different parts of the boundary are defined by different formulae, or when different types of the boundary or interface conditions are specified at different parts of the boundary. A piece-wise parametrization will require separate bases of the type (40a) for individual segments of the boundary. In this case, a natural choice may be to replace the trigonometric functions (39) with Chebyshev polynomials; other possibilities will be investigated as well.

Yet another direction for future work will be to allow for multiple sub-regions, for example, multiple scatterers immersed into the same background medium. The simplest case will amount to considering a piece-wise constant function $k^2(x, y)$ in the Helmholtz equation (9), while more elaborate settings may also include the variation of material characteristics [both ε and k, see (89)] inside each individual scatterer. We will still assume that sharp variations are allowed only at the boundaries/interfaces, whereas inside each individual subregion the functions $\varepsilon(x, y)$ and $k^2(x, y)$ vary smoothly. This keeps the overall problem predominantly smooth. The method of difference potentials has previously been applied to multiple subregions in the context of active noise control, see [34]. Its application to solving the reflection/transmission problems for multiple scattering will be similar.

Applying the proposed methodology to 3D wave propagation will be more involved. While all the fundamental concepts and constructs described in the paper, such as Calderon operators and their properties, remain the same in 3D, a number of changes throughout the entire numerical procedure will still be required. In particular, the coordinates associated with the curve that we have introduced in Appendix A in order to build the equation-based

extension will need to be replaced with surface-oriented coordinates, see [21]. The only type of solvers for the AP that seem feasible in 3D are iterative solvers, and we plan to use the Krylov-type algorithm Risolv of [52] with complex-shifted preconditioners [13–16] applied with the help of multigrid.

The extension of the proposed methodology to time-dependent problems (e.g., the wave, i.e., d'Alembert, equation instead of the Helmholtz equation) will require additional theoretical developments. Two types of methods that have been introduced and analyzed previously can prove useful in this context: the methods for unsteady control of sound [59], and lacunae-based methods that are used for setting the unsteady ABCs [44, 56, 58], as well as for achieving the improved performance over long times [35–37].

We also note that even though both our current implementation and future directions focus on wave propagation problems, the method of difference potentials is capable of addressing a considerably broader range of formulations, including problems in heat transfer, elasticity, fluid dynamics, and other areas, see [42].

Acknowledgements Work supported by the US NSF under grant # DMS-0810963, US–Israel Binational Science Foundation (BSF) under grant # 2008094, US AFOSR under grant # FA9550-10-1-0092, and US ARO under grant # W911NF-11-1-0384.

Appendix A: Coordinates Associated with a Curve and Equation-Based Extension

A.1 Elliptical Coordinates

Let Γ be an ellipse with semi-axes a and b:

$$\frac{x^2}{a^2}+\frac{y^2}{b^2}=1. \tag{69}$$

Then, the equation-based extension (introduced in Sect. 4.2 for the case of a circle) is convenient to build using the elliptical coordinates.

Denote $d=\sqrt{a^2-b^2}$ the distance from the center of the ellipse (69) to either of its foci. A common definition of elliptical coordinates (η,φ) is given by:

$$\begin{cases} x = d\cosh\eta\cos\varphi, \\ y = d\sinh\eta\sin\varphi, \end{cases} \tag{70}$$

where $\eta\geq 0$ and $\varphi\in[0,2\pi)$. The coordinate lines that correspond to (70) are families of ellipses and hyperbolas on the plane, see Fig. 7. For a fixed $\eta=\eta_0$, the coordinate line is an ellipse:

$$\frac{x^2}{d^2\cosh^2\eta_0}+\frac{y^2}{d^2\sinh^2\eta_0}=1,$$

so that the original ellipse (69) corresponds to

$$\eta_0=\frac{1}{2}\ln\frac{a+b}{a-b}. \tag{71}$$

For a fixed $\varphi=\varphi_0$, the coordinate line is a hyperbola:

$$\frac{x^2}{d^2\cos^2\varphi_0}-\frac{y^2}{d^2\sin^2\varphi_0}=\cosh^2\eta-\sinh^2\eta=1.$$

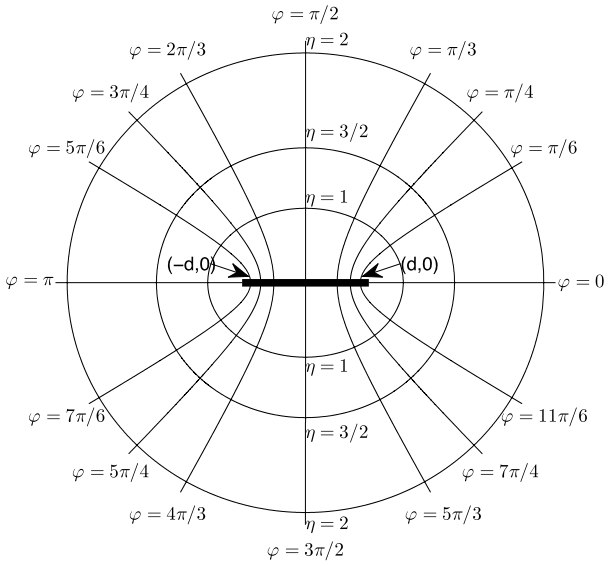

Fig. 7 Elliptical coordinates

The basis vectors for elliptical coordinates are (see Fig. 7):

$$\boldsymbol{e}_1 \equiv \hat{\eta} = \frac{\partial \boldsymbol{r}}{\partial \eta} = (d \sinh\eta \cos\varphi, d \cosh\eta \sin\varphi)$$

and

$$\boldsymbol{e}_2 \equiv \hat{\varphi} = \frac{\partial \boldsymbol{r}}{\partial \varphi} = (-d \cosh\eta \sin\varphi, d \sinh\eta \cos\varphi),$$

where $\boldsymbol{r} = (x, y)$ is the radius-vector defined via (70). Hence, the Lame coefficients are equal to one another:

$$H_1 \equiv H_\eta = |\boldsymbol{e}_1| = d\sqrt{\sinh^2\eta + \sin^2\varphi} = |\boldsymbol{e}_2| = H_2 \equiv H_\varphi. \tag{72}$$

Accordingly, the Helmholtz equation (9) in the elliptical coordinates (70) transforms into

$$\frac{1}{H^2}\left[\frac{\partial^2 u}{\partial \eta^2} + \frac{\partial^2 u}{\partial \varphi^2}\right] + k^2(\eta, \varphi)u = f, \tag{73}$$

where $H = H_\eta = H_\varphi$, see formula (72).

Suppose that $\boldsymbol{\xi}_\Gamma = (\xi_0, \xi_1)|_\Gamma$ is given on the ellipse (69) so that $\xi_0 = \xi_0(\varphi)$ and $\xi_1 = \xi_1(\varphi)$. In the vicinity of this ellipse, we define a new smooth function $v = v(\eta, \varphi)$ by means of the Taylor formula [cf. formula (42)]:

$$v(\eta, \varphi) = v(\eta_0, \varphi) + \sum_{l=1}^{L} \frac{1}{l!} \frac{\partial^l v(\eta_0, \varphi)}{\partial \eta^l} (\eta - \eta_0)^l, \tag{74}$$

where η_0 is given by expression (71), and the choice of L is discussed in Sect. 4.3. The zeroth and first order derivatives in formula (74) are obtained by requiring that [cf. formula (43)]

$$v(\eta_0, \varphi) = \xi_0(\varphi) \quad \text{and} \quad \frac{\partial v(\eta_0, \varphi)}{\partial \eta} = \xi_1(\varphi). \tag{75}$$

Note that whereas in polar coordinates $\frac{\partial v}{\partial n} = \frac{\partial v}{\partial r}$, in elliptical coordinates we have: $\frac{\partial v}{\partial n} = \frac{1}{H}\frac{\partial v}{\partial \eta}$. The higher order derivatives for formula (74) are obtained via equation-based differentiation:

$$\begin{aligned}
\frac{\partial^2 u}{\partial \eta^2} &= H^2 f - \frac{\partial^2 u}{\partial \varphi^2} - H^2 k^2 u = H^2 f - \frac{\partial^2 \xi_0}{\partial \varphi^2} - H^2 k^2 \xi_0, \\
\frac{\partial^3 u}{\partial \eta^3} &= 2H\frac{\partial H}{\partial \eta} f + H^2 \frac{\partial f}{\partial \eta} - \frac{\partial^3 u}{\partial \eta \partial \varphi^2} - 2\left(H\frac{\partial H}{\partial \eta}k^2 u + H^2 k \frac{\partial k}{\partial \eta}\right)u - H^2 k^2 \frac{\partial u}{\partial \eta} \\
&= 2H\frac{\partial H}{\partial \eta} f + H^2 \frac{\partial F}{\partial \eta} - \frac{\partial^2 \xi_1}{\partial \varphi^2} - 2\left(H\frac{\partial H}{\partial \eta}k^2 + H^2 k \frac{\partial k}{\partial \eta}\right)\xi_0 - H^2 k^2 \xi_1,
\end{aligned}$$

and

$$\begin{aligned}
\frac{\partial^4 u}{\partial \eta^4} &= 2\left(\left(\frac{\partial H}{\partial \eta}\right)^2 + H\frac{\partial^2 H}{\partial \eta^2}\right) f + 4H\frac{\partial H}{\partial \eta}\frac{\partial f}{\partial \eta} + H^2 \frac{\partial^2 f}{\partial \eta^2} - \frac{\partial^4 u}{\partial \eta^2 \partial \varphi^2} \\
&\quad - 2\left(\left(\left(\frac{\partial H}{\partial \eta}\right)^2 + H\frac{\partial^2 H}{\partial \eta^2}\right)k^2 + 4H\frac{\partial H}{\partial \eta}k\frac{\partial k}{\partial \eta} + H^2 k\frac{\partial^2 k}{\partial \eta^2} + H^2\left(\frac{\partial k}{\partial \eta}\right)^2\right)u \\
&\quad - 4\left(H\frac{\partial H}{\partial \eta}k^2 + H^2 k\frac{\partial k}{\partial \eta}\right)\frac{\partial u}{\partial \eta} - H^2 k^2 \frac{\partial^2 u}{\partial \eta^2} \\
&= 2\left(\left(\frac{\partial H}{\partial \eta}\right)^2 + H\frac{\partial^2 H}{\partial \eta^2}\right) f + 4H\frac{\partial H}{\partial \eta}\frac{\partial f}{\partial \eta} + H^2 \frac{\partial^2 f}{\partial \eta^2} - \frac{\partial^4 u}{\partial \eta^2 \partial \varphi^2} \\
&\quad - 2\left(\left(\left(\frac{\partial H}{\partial \eta}\right)^2 + H\frac{\partial^2 H}{\partial \eta^2}\right)k^2 + 4H\frac{\partial H}{\partial \eta}k\frac{\partial k}{\partial \eta} + H^2 k\frac{\partial^2 k}{\partial \eta^2} + H^2\left(\frac{\partial k}{\partial \eta}\right)^2\right)\xi_0 \\
&\quad - 4\left(H\frac{\partial H}{\partial \eta}k^2 + H^2 k\frac{\partial k}{\partial \eta}\right)\xi_1 - H^2 k^2\left(H^2 f - \frac{\partial^2 \xi_0}{\partial \varphi^2} - H^2 k^2 \xi_0\right),
\end{aligned}$$

where

$$\begin{aligned}
\frac{\partial^4 u}{\partial \varphi^2 \partial \eta^2} &= 2\left(\left(\frac{\partial H}{\partial \varphi}\right)^2 + H\frac{\partial^2 H}{\partial \varphi^2}\right) f + 4H\frac{\partial H}{\partial \varphi}\frac{\partial f}{\partial \varphi} + H^2 \frac{\partial^2 f}{\partial \varphi^2} - \frac{\partial^4 u}{\partial \varphi^4} \\
&\quad - 2\left(\left(\left(\frac{\partial H}{\partial \varphi}\right)^2 + H\frac{\partial^2 H}{\partial \varphi^2}\right)k^2 + 4H\frac{\partial H}{\partial \varphi}k\frac{\partial k}{\partial \varphi} + H^2 k\frac{\partial^2 k}{\partial \varphi^2} + H^2\left(\frac{\partial k}{\partial \varphi}\right)^2\right)u \\
&\quad - 4\left(H\frac{\partial H}{\partial \varphi}k^2 + H^2 k\frac{\partial k}{\partial \varphi}\right)\frac{\partial u}{\partial \varphi} - H^2 k^2 \frac{\partial^2 u}{\partial \varphi^2} \\
&= 2\left(\left(\frac{\partial H}{\partial \varphi}\right)^2 + H\frac{\partial^2 H}{\partial \varphi^2}\right) f + 4H\frac{\partial H}{\partial \varphi}\frac{\partial f}{\partial \varphi} + H^2 \frac{\partial^2 f}{\partial \varphi^2} - \frac{\partial^4 \xi_0}{\partial \varphi^4} \\
&\quad - 2\left(\left(\left(\frac{\partial H}{\partial \varphi}\right)^2 + H\frac{\partial^2 H}{\partial \varphi^2}\right)k^2 + 4H\frac{\partial H}{\partial \varphi}k\frac{\partial k}{\partial \varphi} + H^2 k\frac{\partial^2 k}{\partial \varphi^2} + H^2\left(\frac{\partial k}{\partial \varphi}\right)^2\right)\xi_0 \\
&\quad - 4\left(H\frac{\partial H}{\partial \varphi}k^2 + H^2 k\frac{\partial k}{\partial \varphi}\right)\frac{\partial \xi_0}{\partial \varphi} - H^2 k^2 \frac{\partial^2 \xi_0}{\partial \varphi^2}.
\end{aligned}$$

The function $v(\eta,\varphi)$ of (74) evaluated at the nodes of the grid boundary γ is called the equation-based extension of $\boldsymbol{\xi}_\Gamma$ from the ellipse Γ given by (69) to γ [cf. formula (48)]:

$$\xi_\gamma = \boldsymbol{Ex}\boldsymbol{\xi}_\Gamma \stackrel{\text{def}}{=} v(\eta,\varphi)|_\gamma.$$

A.2 General Case

Equation-based extensions can also be built without assuming any special regular shape of Γ, such as a circle or an ellipse. Suppose that Γ is a general non-self-intersecting smooth closed curve on the plane, and that it is parameterized by its arc length s:

$$\Gamma = \big\{\boldsymbol{R}(s)|0 \le s \le S\big\},$$

where $\boldsymbol{R}$ is the radius-vector that traces the curve. Assume for definiteness that as s increases the point $\boldsymbol{R}(s)$ moves counterclockwise along Γ. The unit tangent vector to Γ is given by

$$\boldsymbol{\tau} = \boldsymbol{\tau}(s) = \frac{d\boldsymbol{R}}{ds}. \tag{76}$$

In addition to the unit tangent, we also consider the unit normal to the curve Γ:

$$\boldsymbol{\nu} = (\nu_x, \nu_y) = (\tau_y, -\tau_x). \tag{77}$$

Given a counterclockwise parametrization $\boldsymbol{R} = \boldsymbol{R}(s)$, the normal $\boldsymbol{\nu}$ of (77) will always be pointing outward with respect to the domain Ω, and hence the pair of vectors $(\boldsymbol{\nu},\boldsymbol{\tau})$ will always have a fixed right-handed orientation on the plane.

Note, that there is a simple relation between the tangent (76), the normal (77), and the curvature κ of the curve Γ. It is given by the Frenet formula:

$$\frac{d\boldsymbol{\tau}}{ds} = \kappa\boldsymbol{\nu}. \tag{78}$$

The vector $\frac{d\boldsymbol{\tau}}{ds}$ is directed toward the center of curvature, i.e., it may point either toward Ω or away from Ω depending on which direction the curve bends. Since the normal (77) has a fixed orientation, the curvature $\kappa = \kappa(s)$ in formula (78) should be taken with the sign (see, e.g., [32, Part 1]):

$$\kappa(s) = \begin{cases} |\frac{d\boldsymbol{\tau}}{ds}|, & \text{if } \frac{d\boldsymbol{\tau}}{ds}\cdot\boldsymbol{\nu} > 0, \\ -|\frac{d\boldsymbol{\tau}}{ds}|, & \text{if } \frac{d\boldsymbol{\tau}}{ds}\cdot\boldsymbol{\nu} < 0. \end{cases} \tag{79}$$

We can now define *the coordinates associated with the curve* Γ. First, we re-emphasize that since Γ is smooth, both the tangent $\boldsymbol{\tau} = \boldsymbol{\tau}(s)$ and the normal $\boldsymbol{\nu} = \boldsymbol{\nu}(s)$ are smooth functions of s. Consider a point on the plane, which is a given node from the grid boundary γ. Draw *the shortest normal* from this point onto the curve Γ. Suppose that the value of the parameter of the curve at the foot of this normal is s, and the distance between the original point and the foot of the normal is n, see Fig. 8. As the position of the point may be on either side of the curve, the value of the distance n is taken with the sign: $n > 0$ corresponds to the positive direction $\boldsymbol{\nu}$, i.e., to the exterior of Ω, and $n < 0$ corresponds to the negative direction of $\boldsymbol{\nu}$, i.e., to the interior of Ω. The pair of numbers (n, s) provides the coordinates that identify the location of a given point on the plane. These coordinates are obviously orthogonal.

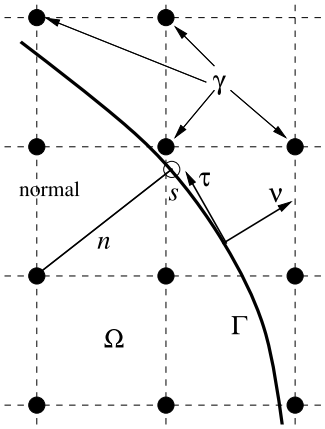

Fig. 8 New coordinates (n, s) and equation-based extension

A limitation of the coordinates (n, s) is that for a general shape of the boundary Γ there may be some ambiguity, as it is possible that multiple shortest normals will exist for a given node. Hence, the distance function will be multi-valued and not differentiable w.r.t. the arc length s. This may happen, in particular, when the boundary Γ has a "cavity". An obvious sufficient condition that avoids such ambiguities is to require that the coordinates (n, s) be used only inside a curvilinear strip of width $2\bar{R}$ that straddles Γ, where $\bar{R} = \min_s R(s)$ is the minimum radius of curvature. In other words, we require that if $\frac{d\boldsymbol{\tau}}{ds} \cdot \boldsymbol{\nu} > 0$ then $n < \bar{\kappa}^{-1} \equiv \bar{R}$, and if $\frac{d\boldsymbol{\tau}}{ds} \cdot \boldsymbol{\nu} < 0$ then $n > \bar{\kappa}^{-1} \equiv -\bar{R}$. This limitation, however, is not severe, because we use the coordinates (n, s) only for the points of the grid boundary γ, which are all about one grid size h away from the curve Γ, see Figs. 3 and 8. Having multiple shortest distances for a given node would then imply that the minimum radius of curvature $\bar{R}$ is also of order h. This means, in turn, that the grid does not adequately resolve the geometry, and needs to be refined. Let us also note that the simulations in this paper, see Sect. 5, do not involve any shapes with potential cavities, i.e., non-convex features with the curvature $\kappa \sim h^{-1}$. In the future, we will analyze shapes with "small" features.

The coordinates (n, s) are orthogonal but not orthonormal. For a given point (n, s), its radius-vector $\boldsymbol{r}$ is expressed as follows:

$$\begin{aligned}\boldsymbol{r} = \boldsymbol{r}(n, s) = \boldsymbol{R}(s) + n\boldsymbol{\nu}(s) &= \big(R_x(s) + n\nu_x(s),\, R_y(s) + n\nu_x(s)\big) \\ &= \left(R_x + n\frac{dR_y}{ds},\, R_y - n\frac{dR_x}{ds}\right),\end{aligned}$$

and consequently, the basis vectors are given by

$$\boldsymbol{e}_1 = \frac{\partial \boldsymbol{r}}{\partial n} = \left(\frac{dR_y}{ds}, -\frac{dR_x}{ds}\right) = (\tau_y, -\tau_x) = \boldsymbol{\nu}$$

and

$$\begin{aligned}\boldsymbol{e}_2 = \frac{\partial \boldsymbol{r}}{\partial s} &= \left(\frac{dR_x}{ds} + n\frac{d^2R_y}{ds^2}, \frac{dR_y}{ds} - n\frac{d^2R_x}{ds^2}\right) \\ &= \left(\frac{dR_x}{ds} + n\kappa\nu_y, \frac{dR_y}{ds} - n\kappa\nu_x\right) \\ &= (\tau_x - n\kappa\tau_x, \tau_y - n\kappa\tau_y) = (1 - n\kappa)\boldsymbol{\tau},\end{aligned}$$

where we have used formulae (76), (77), (78), and (79). Accordingly, the Lame coefficients for the coordinates (n, s) are

$$H_1 \equiv H_n = |\boldsymbol{e}_1| = 1$$

and

$$H_2 \equiv H_s = |\boldsymbol{e}_2| = |1 - n\kappa| = 1 - n\kappa, \tag{80}$$

where the last equality in (80) holds because $n < \kappa^{-1}$ for $\kappa > 0$ and $n > \kappa^{-1}$ for $\kappa < 0$.

In the coordinates (n, s), (9) becomes

$$\frac{1}{H_s}\left[\frac{\partial}{\partial n}\left(H_s\frac{\partial u}{\partial n}\right) + \frac{\partial}{\partial s}\left(\frac{1}{H_s}\frac{\partial u}{\partial s}\right)\right] + k^2(n, s)u = f, \tag{81}$$

where $H_s = H_s(n, s)$ is given by (80), and where we have taken into account that $H_n \equiv 1$. Equation (81) will be used for building the equation-based extension of a given $\boldsymbol{\xi}_\Gamma$ from the continuous boundary Γ to the nodes of the grid boundary γ similar to how the polar Helmholtz equation (41) was used in Sect. 4.2 for building the corresponding extension from the circle.

Note, that if Γ is a circle of radius R, then the foregoing general constructs transform into the corresponding constructs for polar coordinates described in Sect. 4.2. Indeed, in this case the curvature κ of (79) does not depend on s:

$$\kappa = -\frac{1}{R},$$

and consequently [see formula (80)],

$$H_s = 1 + \frac{n}{R} = \frac{R + n}{R} = \frac{r}{R}.$$

Then, according to (81) we can write:

$$\Delta u = \frac{R}{r}\left[\frac{\partial}{\partial n}\left(\frac{r}{R}\frac{\partial u}{\partial n}\right) + \frac{\partial}{\partial s}\left(\frac{R}{r}\frac{\partial u}{\partial s}\right)\right] = \frac{1}{r}\frac{\partial}{\partial n}\left(r\frac{\partial u}{\partial n}\right) + \frac{R^2}{r^2}\frac{\partial^2 u}{\partial s^2}.$$

Finally, we have $n = r - R$ so that $\frac{\partial}{\partial n} = \frac{\partial}{\partial r}$, and $s = R\theta$ so that $\frac{\partial}{\partial s} = \frac{1}{R}\frac{\partial}{\partial \theta}$, which yields:

$$\Delta u = \frac{1}{r}\frac{\partial}{\partial r}\left(r\frac{\partial u}{\partial r}\right) + \frac{1}{r^2}\frac{\partial^2 u}{\partial \theta^2}.$$

Let $\boldsymbol{\xi}_\Gamma = (\xi_0(s), \xi_1(s))$ be given on Γ. In the vicinity of Γ, we define a new smooth function $v = v(n, s)$ by means of the Taylor formula [cf. formula (42)]:

$$v(n, s) = v(0, s) + \sum_{l=1}^{L} \frac{1}{l!}\frac{\partial^l v(0, s)}{\partial n^l} n^l. \tag{82}$$

The zeroth and first order derivatives in formula (82) are obtained by requiring that $\boldsymbol{Tr}\, v = \boldsymbol{\xi}_\Gamma$:

$$v(0, s) = \xi_0(s) \quad \text{and} \quad \frac{\partial v(0, s)}{\partial n} = \xi_1(s). \tag{83}$$

All higher order derivatives in formula (82) are determined with the help of equation (81) applied to v. For convenience, we multiply both sides by H_s and then solve for the second derivative with respect to n, which yields:

$$\frac{\partial^2 v}{\partial n^2} = \tilde{f} - \tilde{k}^2(n,s)v - \frac{\partial}{\partial s}\left(\frac{1}{H_s}\frac{\partial v}{\partial s}\right) - \frac{\partial H_s}{\partial n}\frac{\partial v}{\partial n}, \tag{84}$$

where $\tilde{k} = H_s k$, $\tilde{f} = H_s f$, and $\frac{\partial H_s}{\partial n} = -\kappa(s)$, see formula (80). Consequently,

$$\frac{\partial^2 v(0,s)}{\partial n^2} = \tilde{f}(0,s) - \tilde{k}^2(0,s)\xi_0(s) - \frac{\partial}{\partial s}\left(\frac{1}{H_s}\frac{\partial \xi_0(s)}{\partial s}\right) + \kappa(s)\xi_1(s). \tag{85}$$

Next, we differentiate equation (84) with respect to n:

$$\frac{\partial^3 v}{\partial n^3} = \frac{\partial \tilde{f}}{\partial n} - \frac{\partial \tilde{k}^2}{\partial n}v - \tilde{k}^2\frac{\partial v}{\partial n} - \frac{\partial}{\partial s}\left(\frac{\partial H_s^{-1}}{\partial n}\frac{\partial v}{\partial s}\right) - \frac{\partial}{\partial s}\left(\frac{1}{H_s}\frac{\partial}{\partial s}\left[\frac{\partial v}{\partial n}\right]\right) + \kappa\frac{\partial^2 v}{\partial n^2}, \tag{86}$$

and substituting $v(0,s)$ and $\frac{\partial v(0,s)}{\partial n}$ from (83) and $\frac{\partial^2 v(0,s)}{\partial n^2}$ from (85), we obtain $\frac{\partial^3 v(0,s)}{\partial n^3}$. Similarly, the fourth normal derivative $\frac{\partial^4 v(0,s)}{\partial n^4}$ can be evaluated by differentiating equation (86) with respect to n:

$$\begin{aligned}\frac{\partial^4 v}{\partial n^4} = {} & \frac{\partial^2 \tilde{f}}{\partial n^2} - \frac{\partial^2 \tilde{k}^2}{\partial n^2}v - \frac{\partial \tilde{k}^2}{\partial n}\frac{\partial v}{\partial n} - \frac{\partial}{\partial s}\left(\frac{\partial^2 H_s^{-1}}{\partial n^2}\frac{\partial v}{\partial s}\right) \\ & - 2\frac{\partial}{\partial s}\left(\frac{\partial H_s^{-1}}{\partial n}\frac{\partial}{\partial s}\left[\frac{\partial v}{\partial n}\right]\right) - \frac{\partial}{\partial s}\left(\frac{1}{H_s}\frac{\partial}{\partial s}\left[\frac{\partial^2 v}{\partial n^2}\right]\right) + \kappa\frac{\partial^3 v}{\partial n^3},\end{aligned}$$

and then substituting the previously computed derivatives $v(0,s)$, $\frac{\partial v(0,s)}{\partial n}$, $\frac{\partial^2 v(0,s)}{\partial n^2}$, and $\frac{\partial^3 v(0,s)}{\partial n^3}$. Higher order derivatives (e.g., for the sixth order scheme) can be obtained in the same manner.

As in (42), we emphasize that formula (82) is not an approximation of a given $v(n,s)$ by its truncated Taylor's expansion. Rather it is the definition of a new function $v(n,s)$. This function is used for building the equation-based extension of $\boldsymbol{\xi}_\Gamma$ from Γ to γ:

$$\xi_\gamma = \boldsymbol{Ex}\boldsymbol{\xi}_\Gamma \stackrel{\text{def}}{=} v(n,s)|_\gamma. \tag{87}$$

So, extension (87) is obtained by drawing a normal from a given node of γ to Γ, see Fig. 8, and then using the Taylor formula with higher order derivatives computed by differentiating the governing equation (81). If Γ is a circle, then the derivatives with respect to n in formula (82) become radial derivatives, and accordingly, the extension (87) transforms into (48).

Extension of the right-hand side f is built with the help of the Taylor formula

$$f(n,s) = f(0,s) + \sum_{l=1}^{L-2}\frac{1}{l!}\frac{\partial^l f(0,s)}{\partial n^l}n^l. \tag{88}$$

The derivatives of f that enter into (88) can be computed as one-sided normal derivatives on the interior side of Γ, similarly to how it is done for formula (49) when Γ is a circle.

Note that for more complicated shapes it may often be convenient to have a piece-wise parametrization for the curve Γ as opposed to the global parametrization. Piece-wise parametrization and different bases (40a) for different portions of the boundary (e.g., independent Chebyshev systems) may also pave the way toward discontinuous coefficients in the boundary conditions, non-smooth boundaries, and other formulations which will be analyzed in the future, see Sect. 6.

It should finally be mentioned that a somewhat more elaborate procedure will yield an equation-based extension for an equation more general than (9):

$$\operatorname{div}(\varepsilon \cdot \operatorname{grad} u) + k^2 u = f. \tag{89}$$

In formula (89), $\varepsilon = \varepsilon(x, y)$ is a symmetric and positive definite tensor of rank 2. Equation (9) is a particular case of (89) where ε is the identity. In [6], we have considered another particular case of (89), with ε being diagonal in the Cartesian coordinates: $\varepsilon = \operatorname{diag}\{a, b\}$.

References

1. Babuska, I.M., Sauter, S.A.: Is the pollution effect of the FEM avoidable for the Helmholtz equation considering high wave numbers? SIAM J. Numer. Anal. **34**(6), 2392–2423 (1997)
2. Baruch, G., Fibich, G., Tsynkov, S.: High-order numerical method for the nonlinear Helmholtz equation with material discontinuities in one space dimension. J. Comput. Phys. **227**, 820–850 (2007)
3. Baruch, G., Fibich, G., Tsynkov, S., Turkel, E.: Fourth order scheme for wave-like equations in frequency space with discontinuities in the coefficients. Commun. Comput. Phys. **5**(2–4), 442–455 (2009)
4. Bayliss, A., Goldstein, C.I., Turkel, E.: On accuracy conditions for the numerical computation of waves. J. Comput. Phys. **59**(3), 396–404 (1985)
5. Britt, S., Tsynkov, S., Turkel, E.: A compact fourth order scheme for the Helmholtz equation in polar coordinates. J. Sci. Comput. **45**(1–3), 26–47 (2010)
6. Britt, S., Tsynkov, S., Turkel, E.: Numerical simulation of time-harmonic waves in inhomogeneous media using compact high order schemes. Commun. Comput. Phys. **9**(3), 520–541 (2011)
7. Calderon, A.P.: Boundary-value problems for elliptic equations. In: Proceedings of the Soviet-American Conference on Partial Differential Equations at Novosibirsk, pp. 303–304. Fizmatgiz, Moscow (1963)
8. Cangellaris, A.C., Wright, D.B.: Analysis of the numerical error caused by the stair-stepped approximation of a conducting boundary in FDTD simulations of electromagnetic phenomena. IEEE Trans. Antennas Propag. **39**(10), 1518–1525 (1991)
9. Carey, G.F., Chow, S.S., Seager, M.K.: Approximate boundary-flux calculations. Comput. Methods Appl. Mech. Eng. **50**(2), 107–120 (1985)
10. Collatz, L.: The Numerical Treatment of Differential Equations. Springer, New York (1966)
11. El Guennouni, A., Jbilou, K., Sadok, H.: A block version of BICGSTAB for linear systems with multiple right-hand sides. Electron. Trans. Numer. Anal. **16**, 129–142 (2003) (electronic)
12. Elbouyahyaoui, L., Messaoudi, A., Sadok, H.: Algebraic properties of the block GMRES and block Arnoldi methods. Electron. Trans. Numer. Anal. **33**, 207–220 (2008/09)
13. Erlangga, Y., Turkel, E.: Iterative schemes for high order compact discretizations to the exterior Helmholtz equation. ESAIM: Math. Model. Num. Anal. **46**(3), 647–660 (2012)
14. Erlangga, Y.A., Oosterlee, C.W., Vuik, C.: A novel multigrid based preconditioner for heterogeneous Helmholtz problems. SIAM J. Sci. Comput. **27**(4), 1471–1492 (2006) (electronic)
15. Erlangga, Y.A., Vuik, C., Oosterlee, C.W.: On a class of preconditioners for solving the Helmholtz equation. Appl. Numer. Math. **50**(3–4), 409–425 (2004)
16. Erlangga, Y.A.: Advances in iterative methods and preconditioners for the Helmholtz equation. Arch. Comput. Methods Eng. **15**(1), 37–66 (2008)
17. Freund, R.W., Malhotra, M.: A block QMR algorithm for non-Hermitian linear systems with multiple right-hand sides. In: Proceedings of the Fifth Conference of the International Linear Algebra Society, Atlanta, GA, 1995, vol. 254, pp. 119–157 (1997)
18. Greengard, L., Rokhlin, V.: A fast algorithm for particle simulations. J. Comput. Phys. **73**(2), 325–348 (1987)
19. Gunzburger, M., Peterson, J.: Reduced-order modeling of complex systems with multiple system parameters. In: Large-Scale Scientific Computing. Lecture Notes in Comput. Sci., vol. 3743, pp. 15–27. Springer, Berlin (2006)

20. Harari, I., Turkel, E.: Accurate finite difference methods for time-harmonic wave propagation. J. Comput. Phys. **119**(2), 252–270 (1995)
21. Hirschel, E.H., Kordulla, W.: Shear Flow in Surface-Oriented Coordinates. Notes on Numerical Fluid Mechanics, vol. 4. Vieweg, Braunschweig (1981–1986)
22. Holland, R.: Pitfalls of staircase meshing. IEEE Trans. Electromagn. Compat. **35**, 434–439 (1993)
23. Ihlenburg, F.: Finite Element Analysis of Acoustic Scattering. Applied Mathematical Sciences, vol. 132. Springer, Berlin (1998)
24. Kamenetskii, D.S.: Difference potentials and the parameterization of solutions of homogeneous difference equations. Comput. Math. Math. Phys. **38**(11), 1754–1767 (1998)
25. Kamenetskii, D.S.: Difference generalized Poincaré-Steklov operators and potentials with density from a space of jumps. Comput. Math. Math. Phys. **39**(8), 1275–1282 (1999)
26. Kamenetskii, D.S.: On one form of representing the difference potentials. Appl. Numer. Math. **33**(1–4), 501–508 (2000)
27. Lax, P., Wendroff, B.: Systems of conservation laws. Commun. Pure Appl. Math. **13**, 217–237 (1960)
28. Lele, S.K.: Compact finite difference schemes with spectral like resolution. J. Comput. Phys. **103**, 16–42 (1992)
29. Li, Z., Ito, K.: The Immersed Interface Method: Numerical Solutions of PDEs Involving Interfaces and Irregular Domains. Frontiers in Applied Mathematics, vol. 33. Society for Industrial and Applied Mathematics (SIAM), Philadelphia (2006)
30. Lončarić, J., Ryaben'kii, V.S., Tsynkov, S.V.: Active shielding and control of noise. SIAM J. Appl. Math. **62**(2), 563–596 (2001)
31. Nabavi, M., Siddiqui, K., Dargahi, J.: A new 9-point sixth-order accurate compact finite-difference method for the Helmholtz equation. J. Sound Vib. **307**, 972–982 (2007)
32. Novikov, S.P., Fomenko, A.T.: Basic Elements of Differential Geometry and Topology. Mathematics and its Applications (Soviet Series), vol. 60. Kluwer Academic, Dordrecht (1990). Translated from the Russian by M.V. Tsaplina
33. Peskin, C.S.: The immersed boundary method. Acta Numer. **11**, 479–517 (2002)
34. Peterson, A.W., Tsynkov, S.V.: Active control of sound for composite regions. SIAM J. Appl. Math. **67**(6), 1582–1609 (2007)
35. Petropavlovsky, S.V., Tsynkov, S.V.: Quasi-lacunae of Maxwell's equations. SIAM J. Appl. Math. **71**(4), 1109–1122 (2011)
36. Petropavlovsky, S.V., Tsynkov, S.V.: A non-deteriorating algorithm for computational electromagnetism based on quasi-lacunae of Maxwell's equations. J. Comput. Phys. **231**, 558–585 (2012)
37. Qasimov, H., Tsynkov, S.: Lacunae based stabilization of PMLs. J. Comput. Phys. **227**, 7322–7345 (2008)
38. Reznik, A.A.: Approximation of surface potentials of elliptic operators by difference potentials. Dokl. Akad. Nauk SSSR **263**(6), 1318–1321 (1982)
39. Richtmyer, R.D.: Difference Methods for Initial-Value Problems. Interscience Tracts in Pure and Applied Mathematics, vol. 4. Interscience, New York (1957)
40. Rokhlin, V.: Solution of acoustic scattering problems by means of second kind integral equations. Wave Motion **7**(3), 257–272 (1983)
41. Ryaben'kii, V.S.: Boundary equations with projections. Russ. Math. Surv. **40**(2), 147–183 (1985)
42. Ryaben'kii, V.S.: Method of Difference Potentials and Its Applications. Springer Series in Computational Mathematics, vol. 30. Springer, Berlin (2002)
43. Ryaben'kii, V.S., Filippov, A.F.: On Stability of Difference Equations. Gosudarstv. Izdat. Tehn.-Teor. Lit, Moscow (1956)
44. Ryaben'kii, V.S., Tsynkov, S.V., Turchaninov, V.I.: Global discrete artificial boundary conditions for time-dependent wave propagation. J. Comput. Phys. **174**(2), 712–758 (2001)
45. Ryaben'kii, V.S., Tsynkov, S.V.: A Theoretical Introduction to Numerical Analysis. Chapman & Hall/CRC, Boca Raton (2007)
46. Seeley, R.T.: Singular integrals and boundary value problems. Am. J. Math. **88**, 781–809 (1966)
47. Singer, I., Turkel, E.: High-order finite difference methods for the Helmholtz equation. Comput. Methods Appl. Mech. Eng. **163**(1–4), 343–358 (1998)
48. Singer, I., Turkel, E.: Sixth-order accurate finite difference schemes for the Helmholtz equation. J. Comput. Acoust. **14**(3), 339–351 (2006)
49. Sofronov, I.L.: A new method for the numerical solution of regular elliptic problems. Dokl. Akad. Nauk SSSR **296**(5), 1057–1061 (1987)
50. Strang, G., Fix, G.J.: An Analysis of the Finite Element Method. Prentice Hall, Englewood Cliffs (1973)
51. Sutmann, G.: Compact finite difference schemes of sixth order for the Helmholtz equation. J. Comput. Appl. Math. **203**(1), 15–31 (2007)

52. Tal-Ezer, H., Turkel, E.: The iterative solver Risolv with application to the exterior Helmholtz problem. SIAM J. Sci. Comput. **32**(1), 463–475 (2010)
53. Tolstykh, A.I., Lipavskii, M.V.: On performance of methods with third- and fifth-order compact upwind differencing. J. Comput. Phys. **140**(2), 205–232 (1998)
54. Tsukerman, I.: A class of difference schemes with flexible local approximation. J. Comput. Phys. **211**(2), 659–699 (2006)
55. Tsynkov, S.V.: Numerical solution of problems on unbounded domains: a review. Appl. Numer. Math. **27**(4), 465–532 (1998)
56. Tsynkov, S.V.: Artificial boundary conditions for the numerical simulation of unsteady acoustic waves. J. Comput. Phys. **189**(2), 626–650 (2003)
57. Tsynkov, S.V.: On the definition of surface potentials for finite-difference operators. J. Sci. Comput. **18**(2), 155–189 (2003)
58. Tsynkov, S.V.: On the application of lacunae-based methods to Maxwell's equations. J. Comput. Phys. **199(1)**, 126–149 (2004)
59. Utyuzhnikov, S.V.: Non-stationary problem of active sound control in bounded domains. J. Comput. Appl. Math. **234**(6), 1725–1731 (2010)